Hahn-Meitner-Institut
Berlin

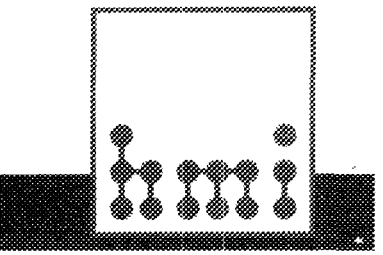

Study of ternary and quaternary spontaneous fission of ^{252}Cf with the NESSI detector

V.G. Tishchenko*, U. Jahnke, C.-M. Herbach and D. Hilscher
Hahn-Meitner-Institut, D-14109 Berlin, Germany

Abstract

Ternary and quaternary spontaneous decay of ^{252}Cf was studied with the NESSI detector, a combination of two 4π detectors for charged particles, neutrons and γ-rays. The applied method of particle identification by measuring the energies and relative time-of-flights of the decay products is shown to be very effective for the study of rare decay modes. The energy and angular distributions of the decay products, the associated neutron multiplicities, the total energy of the prompt γ-radiation as well as correlations between the various observables were measured for the first time in a single full-scale experiment. The characteristics of ternary fission known from previous investigations are confirmed in the frame of a methodically independent experiment. Preliminary estimates of the quaternary fission yield are presented. An attempt is made to determine the mechanism of quaternary fission.

HMI-B 588

November 2002

Berichte des Hahn-Meitner-Instituts (HMI-B)

Das Hahn-Meitner-Institut Berlin GmbH gibt eine Serie von Berichten heraus, in der Forschungs- und Entwicklungsergebnisse des Instituts mitgeteilt werden.
Sie können von der Zentralbibliothek angefordert werden.

Die Berichte werden in die entsprechenden Datenbanken der Fachinformationszentren aufgenommen.

Reports of the Hahn-Meitner-Institute (HMI-B)

The Hahn-Meitner-Institute Berlin GmbH publishes a series of reports, in which research results are reported. The reports may be requested from the library.

The reports are announced to corresponding data bases of the special information centres.

ISSN 0936-0891

Hahn-Meitner-Institut Berlin GmbH · Glienicker Straße 100 · D-14109 Berlin · Telefon: (030) 80 62-1 · Telefax: (030) 80 62-2181

Study of ternary and quaternary spontaneous fission of ^{252}Cf with the NESSI detector

V.G. Tishchenko*, U. Jahnke, C.-M. Herbach and D. Hilscher
Hahn-Meitner-Institut, D-14109 Berlin, Germany

Abstract

Ternary and quaternary spontaneous decay of ^{252}Cf was studied with the NESSI detector, a combination of two 4π detectors for charged particles, neutrons and γ-rays. The applied method of particle identification by measuring the energies and relative time-of-flights of the decay products is shown to be very effective for the study of rare decay modes. The energy and angular distributions of the decay products, the associated neutron multiplicities, the total energy of the prompt γ-radiation as well as correlations between the various observables were measured for the first time in a single full-scale experiment. The characteristics of ternary fission known from previous investigations are confirmed in the frame of a methodically independent experiment. Preliminary estimates of the quaternary fission yield are presented. An attempt is made to determine the mechanism of quaternary fission.

HMI-B 588

Study of ternary and quaternary spontaneous fission of ^{252}Cf with the NESSI detector

V.G. Tishchenko*, U. Jahnke, C.-M. Herbach and D. Hilscher
Hahn-Meitner-Institut, D-14109 Berlin, Germany

Abstract

Ternary and quaternary spontaneous decay of ^{252}Cf was studied with the NESSI detector, a combination of two 4π detectors for charged particles, neutrons and γ-rays. The applied method of particle identification by measuring the energies and relative time-of-flights of the decay products is shown to be very effective for the study of rare decay modes. The energy and angular distributions of the decay products, the associated neutron multiplicities, the total energy of the prompt γ-radiation as well as correlations between the various observables were measured for the first time in a single full-scale experiment. The characteristics of ternary fission known from previous investigations are confirmed in the frame of a methodically independent experiment. Preliminary estimates of the quaternary fission yield are presented. An attempt is made to determine the mechanism of quaternary fission.

Introduction

Normally spontaneous fission of an atomic nucleus is a binary process, in which two heavy fragments originate and, usually, a number of neutrons. Once in several hundred fissions, a third charged particle (CP) is emitted along with two fission fragments. This phenomenon was called *charged particle accompanied fission* or *ternary fission.* It was observed for the first time in 1944 by Alvarez and later confirmed in Ref. [1]. Quite soon it became evident that ternary particles originate mostly from the neck zone of the fissioning nucleus at the very late stage of the fission process. Therefore an idea occurred to use ternary particles as spectators of the nuclear fission process to probe the fission dynamics and the scission configuration. A number of experiments were performed mostly driven by the hope to get access with the help of ternary particles to intimate aspects of the nuclear fission process. Enormous efforts were made to measure carefully the energy and angular distributions of ternary particles, the mass and energy distributions of fission fragments as well as correlations between various observables. Unfortunately, the achievement of the final goal was connected with solution of the inverse three-body problem, significantly complicated by the strong Coulomb interaction of ternary fragments, which destroys the primary

*Present address: Joint Institute for Nuclear Research, 141980 Dubna, Russia

information about the scission configuration. In spite of all efforts the final decision in favor of a definite set of initial parameters has not been obtained so far.

Quaternary fission is a potential source of additional information. Unfortunately, this particular decay channel has an extremely low probability. For instance, for ^{252}Cf it amounts to about $\sim 2 \times 10^{-6}$ with respect to binary fission. Such a low yield of quaternary fission complicates significantly the task of experimental investigation of the decay characteristics. To study such a rare phenomenon it is extremely desirable to have a detection system with high geometric efficiency, if possible, close to 4π. One of the most important problems related to the design of 4π detectors concerns the organization of the time trigger for time-of-flight measurements of decay products. The introduction of a separate start-detector reduces considerably the effective solid angle available for particle detection. There are two ways to solve this problem. First of all, to construct a high-aperture (close to 4π) start detector. The present-day experimental technique has, however, not made a big progress in this direction. The second possibility is to develop proper experimental methods, which allow to replace effectively the start-detector. For instance, the similar problem at the 4π speedometer FOBOS has been solved by measuring time-of-flights of decay products with respect to the radio-frequency of the cyclotron [2]. In the NESSI experiments at the COSY accelerator in Jülich the problem with start-detector was solved by setting up the start-detector out of the main experimental facility, directly upstream in the beam [3]. Obviously, neither of this approaches can be used to study spontaneously fissioning nuclei. One needs a completely new approach. Of coarse, one could use the telescope-technique to identify ternary particles, which has been successfully employed in many previous experiments. However, the disadvantage of telescopes is high lower-energy thresholds, which increase rapidly with the charge of particle being identified. Obviously, this approach does not meet our needs, since we would like to move forward in the detection of heavy particles as far as possible. Here we came to another important problem related to the experimental discovery of *true ternary fission.*

The history of experimental search for true ternary fission is not much shorter than the history of nuclear fission itself. It was already in 1941 (three years after the discovery of nuclear fission phenomena in 1938 by Hahn and Stassman [4]) when Present pointed out that the decay of a heavy nucleus into three heavy fragments is even more favorable energetically than binary fission [5]. Unfortunately, all experimental attempts failed to discover true ternary fission in spontaneous and low-energy fission of actinides. Quite possible, that the reason of failure was caused by inadequate experimental methods. For instance, at the very beginning of investigations an attempt was made to detect ternary fragments with the help of three semiconductor detectors, arranged at angles of 120° with respect to each other. The fragments of true ternary fission were believed to fly away at angles of 120°. However, theoretical calculations performed in 1973 by Diehl and Greiner in the frame of the liquid drop model demonstrated [6, 7], that the most preferable shape of fissioning nucleus concerning the fission barrier is a collinear stretched configuration. It is possible, that the central fragment will not gain too high kinetic energy due to the balancing of counteracting Coulomb forces of the outer fragments. Therefore, to detect such a fragment one should use an experimental setup with low thresholds. Unfortunately, this requirement was not even fulfilled in a recent experiment [8]. Thus, true ternary

spontaneous fission cannot be excluded entirely and the experimental challenge to detect such an exotic decay still exists. It is the aim of the present paper to test the experimental method of ternary (and quaternary) particle identification based on time-of-flights and kinetic energies of the decay products measured with a high-efficiency low-threshold experimental setup.

The paper is organized as follows. A brief description of experimental setup is given in the first section. The second section is devoted to the details of data processing and the method of particle identification. The characteristics of ternary fission are analyzed in the third section. The aim of this analysis is twofold. First of all, we would like to compare the characteristics of ternary fission with the results from previous investigations to make sure, that our data are free of significant methodical errors. On the other hand, the confirmation of previous results in this methodically independent experiment is a good test for absence of methodical errors in previous measurements. The second aim is to analyze the range of application of our approach for particle identification. The characteristics of quaternary fission are analyzed in the fourth section.

1 Experimental setup

The NESSI-detector (NEutron Scintillator tank and SIlicon ball) consists of two 4π detectors, the Berlin Neutron Ball (BNB) [9] for neutron detection and the Berlin Silicon Ball (BSiB) [10] for detection of charged particles. BNB is a spherical shell with an inner and outer diameter of 40 cm and 140 cm, respectively, filled with a liquid gadolinium-loaded scintillator. Fission neutrons are detected by slowing them down by elastic collisions with H- and C-atoms and having them finally captured by gadolinium nuclei in about $10\mu s$. The γ-radiation cascade released from each capture event produces scintillations which are detected by 24 fast photomultipliers distributed on the outer surface of the tank. This *delayed* light component is exploited to count the number of neutrons on an event-by-event basis for each reaction. This number is the essential observable of the BNB detector. The *prompt* component of the total BNB signal originates from prompt γ-rays emitted from fission fragments. This component is exploited to measure the total energy of the prompt γ-rays. The prompt component contains a small contribution of the summed kinetic energy of all charged particles produced within the scintillator liquid from the slowing down of neutrons. The light of those highly ionizing particles is strongly quenched compared to low ionizing Compton scattered electrons from γ-rays.

The silicon ball BSiB is centered around the target in the inner vacuum chamber (40 cm diameter) of BNB. BSiB consists of 162 silicon detectors (500 μm thick) arranged to a sphere with a diameter of 20 cm. The BSiB detector is optimized mainly for detection of *light charged-particles* (LCPs) conventionally defined as particles with charges $1 \leq Z \leq 2$. In this experiment BSiB is used for detection of fission fragments as well. In the present experiment 18 silicon detectors were missing for beam in/out, target system, TV-camera, some defect detectors and 6 detectors replaced by telescopes with a special task for beam experiments.

A weak ^{252}Cf source ($\sim$ 30 fissions/s) on a thin (111 μg/cm^2) nickel foil was used in the

experiment. Energy and time-of-flight with the reference to a common time trigger were measured for each charged particle by BSiB. Time trigger in each event was generated by the second detected charged particle. Therefore only the differences TDC_i between time-of-flight of fragments i and 2 were measured with respect to the second particle. Energy calibration of silicon detectors was made using natural α-peaks from various α-sources, ^{241}Am ($E_\alpha = 5.49$ MeV) and ThC, ThC' ($E_\alpha = 6.06$ MeV and 8.78 MeV). The stability of the electronics was controlled on-line by the position of natural α-line of ^{252}Cf. Only events with multiplicity (number of detected charged particles) of two and greater were recorded. A total number of 4×10^7 events of binary fission was collected during four weeks of measurements.

2 Data analysis

The first important task is to identify the decay products. Usually, FFs in ternary fission have the highest values of kinetic energy among all other decay products. Let us sort particles in each event according to measured kinetic energies: $E_1 \geq E_2 \geq \cdots$. Thus, particles 1 and 2 most probably are fission fragments. Their masses can be reconstructed from measured energies applying momentum conservation and taking into account that the total mass of detected fragments should be equal to the mass of the mother nucleus. This task can be easily solved if the mass of ternary particle is known. On the other hand, the identification of the ternary particle is the aim of the analysis. Therefore, let us assume that the ternary particles is an alpha-particle, which is true for the dominating majority of ternary fission events. Later we will check the validity of this assumption. If this assumption turns out to be wrong, we will repeat the mass-reconstruction procedure with another assumption about the type of ternary particle, until we get self-consisting result. In principle, one could use the method of identification of fission fragments based on the analysis of the angular correlation of the decay products. However, we found the approach proposed above to be more efficient, since polar ternary particles and elastic scattering of FFs make the angular analysis insufficient and more complicated.

Let us evaluate now the time-of-flights TOF_1 and TOF_2 of FFs from the thus reconstructed values of their masses and kinetic energies. A parameter, proportional to the time-of-flight of ternary (as well as quaternary) particles can be calculated in the following manner:

$$TOF_3 = TDC_3 + \frac{(TOF_1 - TDC_1) + (TOF_2 - TDC_2)}{2}. \qquad (1)$$

The correlation between the measured energy of the ternary particle E_3 and the parameter TOF_3 is shown in Fig. 1a. Particles of various type can easily be identified with the help of graphical cuts shown in Fig. 1b. Here is the very same place where we can check the validity of the assumptions made above. If the ternary particle hits a wrong window, we repeat the mass reconstruction procedure with another assumptions concerning the type of the ternary particle as well as the choice of candidates for fission fragments. The matrix shown in Fig. 1a is the final result of such a self-consisting procedure.

The absolute calibration of parameter TOF_3 has been done employing long-range alpha particles (LRA). The correlation between parameter TOF_3 and parameter TOF_E,

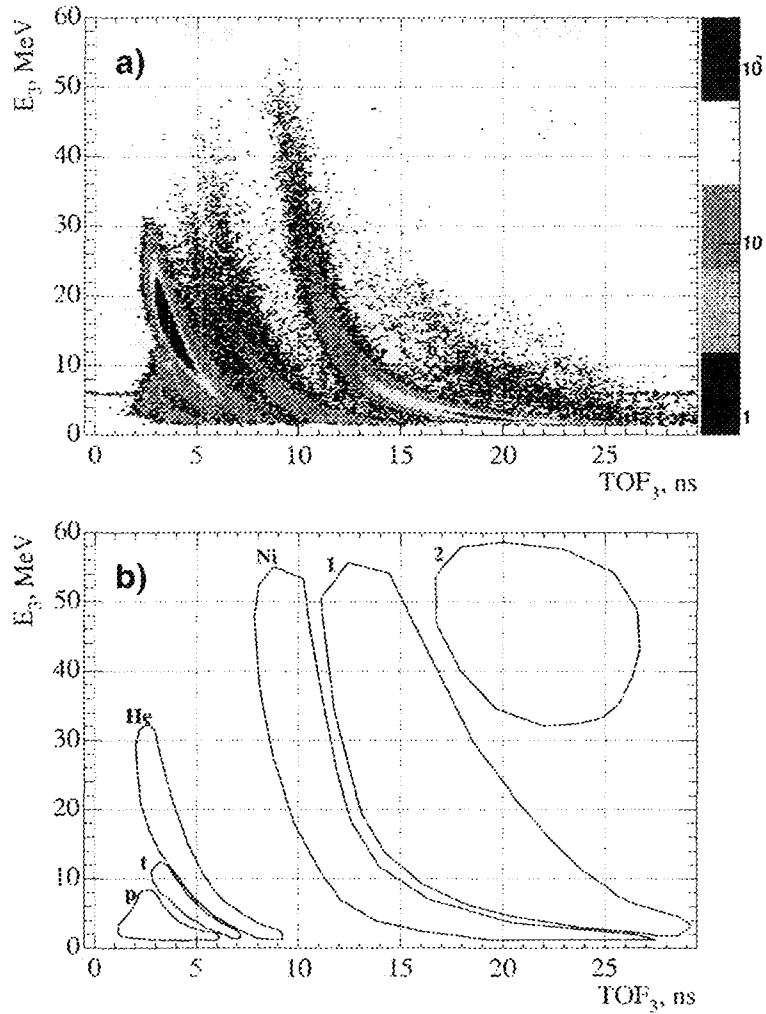

Figure 1: (a) Time-of-flight vs. detected energy of the third particle; (b) graphical windows used for particle identification.

as calculated from the measured energy of α-particles, is shown in Fig. 2a. The calibration coefficients were obtained from linear regression of the data (solid line in Fig. 2a). The distribution of differences of the two parameters ($TOF_E - TOF_3$) is shown in Fig. 2b. The width of this distribution is essentially the total time resolution achieved in the frame of our approach. It amounts to about 570 ps FWHM, which indicates the good quality of both, the experimental data and the mass reconstruction procedure[1].

For pulse-height-defect (PHD) corrections of the measured energy signals an empirical dependence of the total PHD on the fragment mass end energy was used, which was proposed in Ref. [11].

The neutron data were corrected for background measured simultaneously during the experiment. The efficiency correction was determined from binary fission data. The value

[1] the time resolution of a single silicon detector amounts to ~ 250 ps

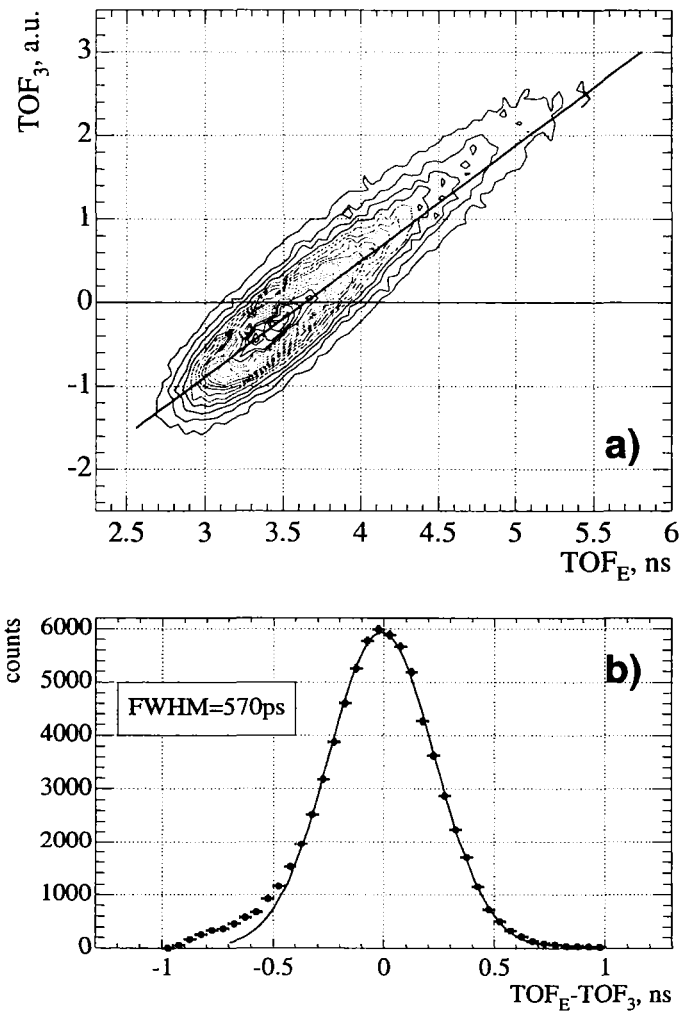

Figure 2: (a) Correlation between time-of-flight of LRA TOF_3 deduced from E-E analysis of fission fragments (see formula 1) and time-of-flight TOF_E calculated from the particle energy; the solid line is the result of linear regression; (b) distribution of the difference of two parameters; the solid line is the result of a Gaussian fit.

of mean the neutron multiplicity in binary fission used as standard is $\overline{\nu} = 3.77$. The deduced detection efficiency for neutrons is $\varepsilon = 0.85$.

The calibration of the gamma-response of BNB was made using binary-fission data. The value of mean total energy of prompt γ-rays for binary fission used as standard is $\overline{E}_\gamma = 7$ MeV.

3 Ternary fission

Let us now analyze the characteristics of various ternary decay modes identified with the help of graphical cuts shown in Fig. 1b. Among hydrogen isotopes (protons and

tritons) we are able to distinguish only non-punch-through particles. Estimated values of punch-through energies of protons, deuterons, tritons, and α-particles amount to 8, 11, 13, and 33 MeV, respectively. Unfortunately, we are not able to distinguish among various helium isotopes. However, it is well known, that helium isotopes in ternary fission are overwhelmingly dominated by α-particles [12]. Therefore, with the help of the selection window "He" (Fig. 1b) we select mainly α-particles. The well-pronounced component marked by window "Ni" corresponds to events of elastic scattering of one of the fission fragments on nickel nuclei from target backing.

3.1 LRA accompanied fission

Events of LRA accompanied fission were selected by window "He" in Fig. 1b. The characteristics of LRA accompanied fission are well-studied by now because of the comparatively high yield of α-particles in spontaneous fission. Therefore, the comparison of our results with the data from literature is a good test of the reliability of the employed approach for particle identification.

3.1.1 The energy of LRAs

The energy spectrum of selected LRA particles is shown in Fig. 3. The contribution from α-particles of spontaneous α-decay of ^{252}Cf is strongly suppressed due to the employment of the time-of-flight parameter for particle identification. A small contribution from random coincidences with these particles is seen in the vicinity of the energy of 6.1 MeV. The results of a Gaussian fit (solid line in Fig. 3a) are shown in the insert of the figure. Comparison of our results with the results of earlier experiments [13, 14] is demonstrated in Fig. 3b. Energy spectra from different measurements were normalized on the yield at the maximum. In the high-energy region all spectra agree quite well, whereas at low energies the disagreement between the results reported by different authors is quite well seen. The low-energy part of the LRA energy spectrum was measured so far quite poorly because of the energy cut caused by shielding foils frequently employed for absorbing α-particles from natural radioactivity of ^{252}Cf. The energy threshold in our approach, as one can see from Fig. 3, amounts to about $2 \div 2.5$ MeV.

3.1.2 The angular distribution of LRAs

The angular distribution of LRA particles is shown in Fig. 4. As can be seen from the figure, most of the detected α-particles are emitted almost perpendicular to the fission axis (so-called *equatorial emission*). The angular distribution has approximately a Gaussian shape. The granularity of the Si-ball does not permit to measure all the details of angular distribution. For a better representation of the experimental data a randomization procedure was applied for coordinates of the impact point inside the hit detector. Experimental data were corrected for the finite size of detectors by deconvoluting the experimental distribution with a Gaussian with the width corresponding to the detector acceptance of $\sigma = 10°$. The result of the deconvolution is shown in Fig. 4 by the solid line. Parameters of the deconvoluted distribution are shown in the insert of the

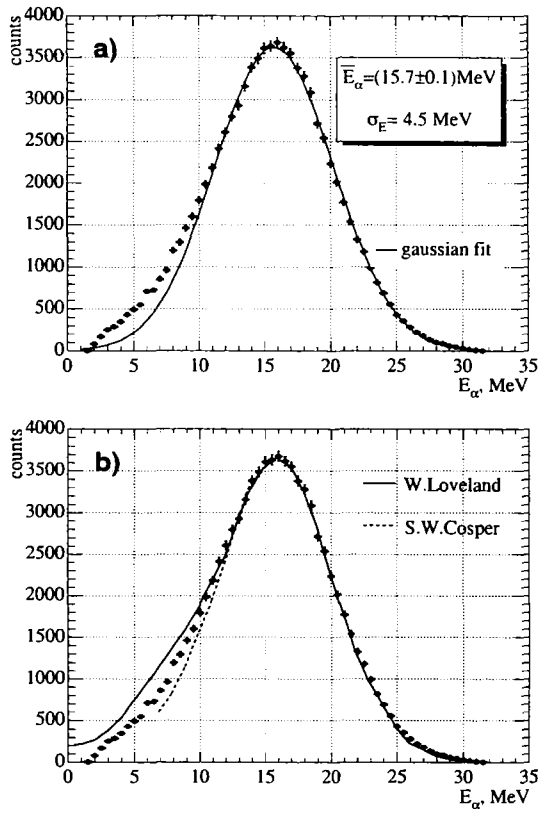

Figure 3: (a) Measured energy spectrum of ternary α-particles (•); the solid line is the result of a Gaussian fit; (b) comparison of our data with the results of W.Loveland [13] (solid line) and S.W.Cosper et al. [14] (dashed line).

figure. The mean emission angle with respect to the light FF obtained from our analysis amounts $84° \pm 1°$. This value is in good agreement with the value of most probable angle of $(84.5° \pm 0.5°)$ recommended in [15]. Precise determination of the parameters of the angular distributions is very important for understanding the mechanism of ternary fission. It is known, that the angular distributions are very sensitive to the choice of the initial parameters for trajectory calculations [16]. Good agreement of our results with the literature data indicates that the granularity of our detection system is sufficient for such kind of measurement.

3.1.3 Evolution of the angular distribution with the kinetic energy of the α-particle

The correlation between the kinetic energy of α-particles and the emission angles with respect to the light fission fragments is shown in Fig. 5. The width of the angular distribution increases with increasing ternary particle kinetic energy. To investigate the characteristics of the angular distribution in more detail we plot in Fig. 6 the mean value and the width of the angular distribution as a function of the kinetic energy. Significant broadening of the angular distribution at high kinetic energies has been also reported in

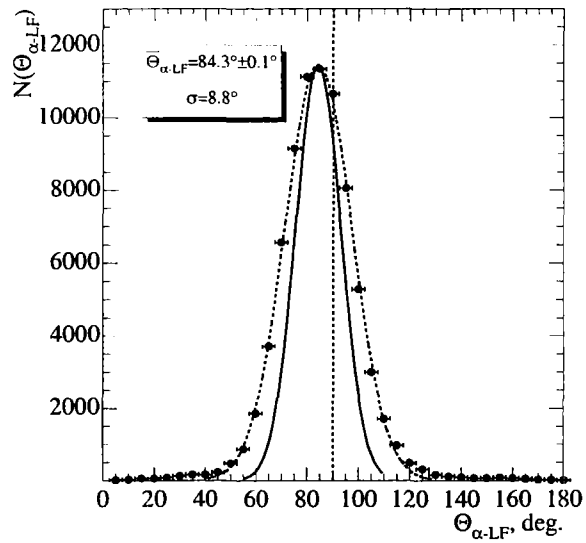

Figure 4: Distribution of angles between α-particle and light fission fragments (•); the dashed line is the result of a Gaussian fit; the solid line is the result of a deconvolution (see text).

earlier works [17, 18]. We observe that at low kinetic energies the width of the angular distribution increases as well. A similar feature was observed in ternary fission of ^{235}U induced by thermal neutrons [19]. An increasing of the mean emission angle with increasing E_α was also reported in Ref. [20, 15]. Possible reasons of the observed correlations were discussed in Ref. [18, 21].

3.1.4 Polar α-particles

A fraction is clearly seen in Fig. 5 of particles emitted in the direction of the velocity vector of FF with a much higher kinetic energy than the mean kinetic energy of LRA. These are so-called *polar α-particles*. An energy spectrum of polar α-particles integrated over angles $(0^\circ \div 35^\circ)$ and $(145^\circ \div 180^\circ)$ is shown in Fig. 7. Parameters of the distribution obtained from a Gaussian fit are shown in the insert of the figure.

One can see two other groups of particles detected at small angles ($\Theta_{\alpha-\mathrm{LF}} < 50^\circ$ and $\Theta_{\alpha-\mathrm{LF}} > 120^\circ$) similar to polar particles, but with considerably lower kinetic energies ($\sim$ 5 MeV). One of the possible models proposed to explain the mechanism of polar particle formation is the evaporation from FFs [22]. The velocity of the emitter is added up to the velocity vector of the evaporated particle. Therefore, particles evaporated in the direction of velocity vector of FF have high kinetic energies in the laboratory frame. And vise-versa, particles emitted in backward direction have small kinetic energies. The expected correlation between the kinetic energy of α-particles emitted from fully accelerated FFs and the emission angles with respect to FFs is shown in Fig. 5 by solid lines. The emission energies of α-particles in the rest frames of light (L) and heavy (H) FFs were taken to be 11 MeV and 14 MeV, respectively. These values were chosen in such

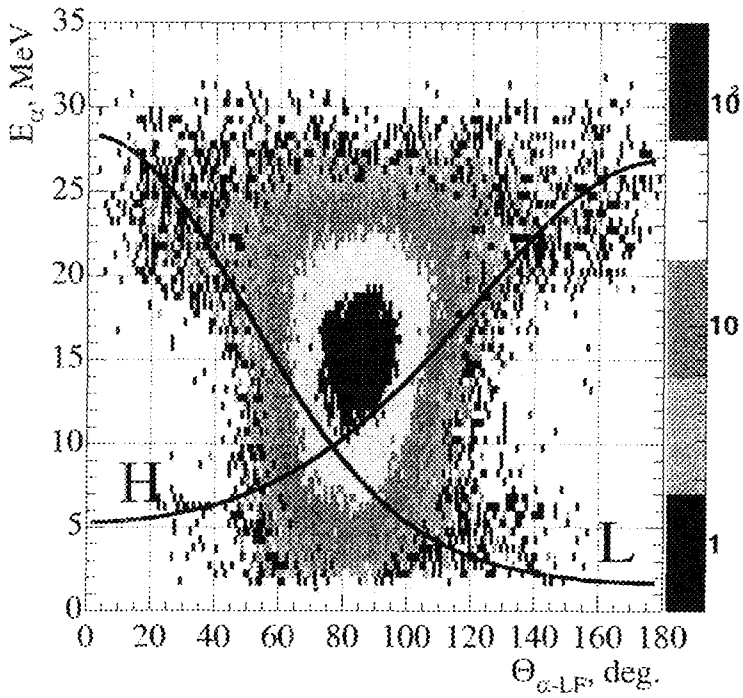

Figure 5: Correlation between the kinetic energy of ternary α-particles and their emission angle with respect to the light fission fragment; solid lines indicate the expected correlation in the case of particle emission from accelerated light (L) and heavy (H) fission fragments.

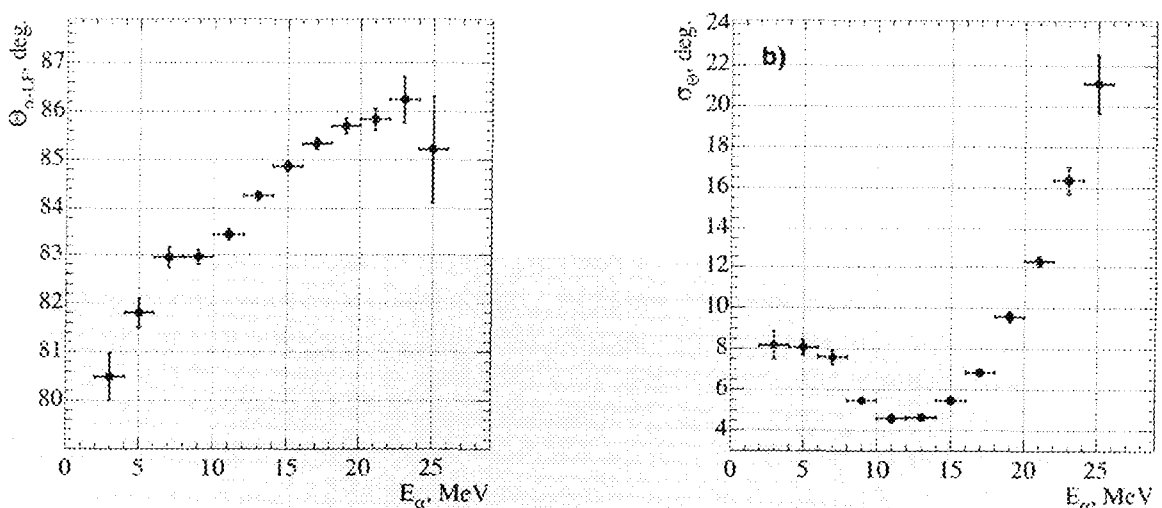

Figure 6: Dependence of mean emission angle (a) and the width of angular distribution (b) on the kinetic energy of LRA.

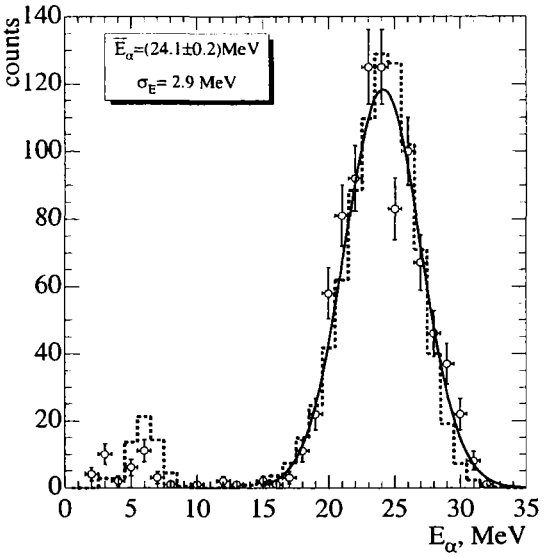

Figure 7: Energy spectrum of polar α-particles emitted at angles $\Theta_{\alpha-\mathrm{LF}} < 50°$ and $\Theta_{\alpha-\mathrm{LF}} > 120°$ (symbols); the solid line is the result of a Gaussian fit; the dashed histogram shows the expected distribution of particles emitted from accelerated FFs.

a way to get a qualitative agreement with experimental data. It is interesting to note, that the lines intersect at $E_\alpha \sim 10$ MeV, that is close to the minimum of the dependence shown in Fig. 6b.

The expected energy spectrum of particles emitted at small angles with respect to FFs is shown in Fig. 7 by the dashed histogram. It was obtained from simple Monte-Carlo simulations taking into account the experimental thresholds.

Thus, the main characteristics of polar α-particles do not contradict the assumption of particle emission from accelerated FFs. Nevertheless, a more detailed analysis is needed to conclude about the mechanism of polar particle formation, which is out of the scope of the present paper.

3.1.5 The associated neutron multiplicity

The energy released in fission is given by the kinetic energy of fission fragments (TKE_{FF}), the kinetic energy of the ternary particle (E_3) and the energy carried off by neutrons and γ-rays. Since we have access to all these components we can study the evolution of these observables with the kinetic energy of ternary particles.

The mean number of emitted neutrons ($\overline{\nu}$) is shown in Fig. 8 as function of the kinetic energy of LRA (solid circles). The approximately linear decrease of $\overline{\nu}$ has been also observed in previous works (see Refs. [23, 24, 25, 26]). At low energies ($E_\alpha < 10$ MeV) we observe $\overline{\nu}$ to be almost independent of α-particle kinetic energy. The low energy region has been poorly studied so far, therefore our data can be considered as a good contribution to the known systematics. The associated neutron multiplicity in polar-alpha accompanied fission is shown in Fig. 8 by open circles. The dash-dotted line at $\overline{\nu} = 3.77$ corresponds

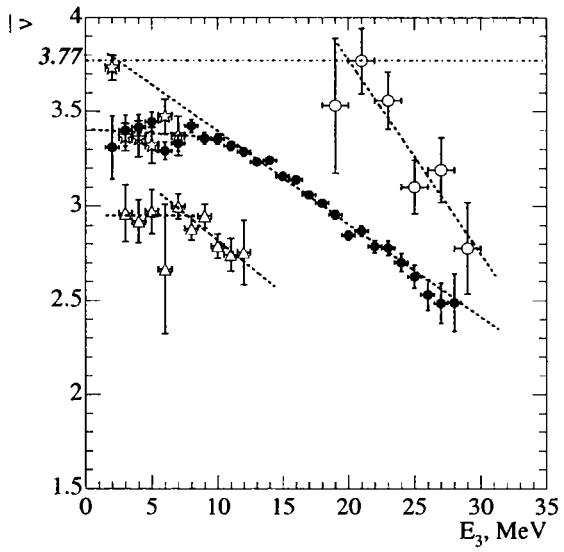

Figure 8: Mean neutron multiplicity as function of the kinetic energy of the ternary particle in LRA (•), polar alpha (○), triton (△), and proton (⋆) accompanied fission.

to the mean neutron multiplicity in binary fission. The dashed lines are the result of linear fits of experimental data. The slope parameters obtained from linear fits are given in Table 1. In the case of equatorial emission the neutron multiplicity is always less than the value in binary fission. The associated neutron multiplicity in polar-α accompanied fission reaches the value observed in binary fission at $E_\alpha \sim 20$ MeV.

3.1.6 The energy of prompt γ-rays

The correlation of the mean total energy of prompt γ-rays ($\overline{E}_\gamma$) and kinetic energy of α-particle is shown in Fig. 9. The dashed-dotted line at $E_\gamma = 7$ MeV shows the mean energy of γ-rays emitted in binary fission. The evolution of $\overline{E}_\gamma$ with E_α is qualitatively similar to the behavior of $\overline{\nu}(E_\alpha)$. In the case of equatorial α-particle emission $\overline{E}_\gamma$ is always less than the value in binary fission and decreases slowly with increasing E_α. The slope of the $\overline{E}_\gamma(E_\alpha)$ dependence is much steeper in the case of polar α emission.

Thus, the average values of neutron multiplicity and energy of prompt γ-rays indicate, that the FFs in LRA accompanied fission are less excited than in binary fission.

3.1.7 The total kinetic energy of fission fragments

The evolution of the average total kinetic energy of FFs with E_α is shown in Fig. 10. At very low kinetic energies of ternary particles the TKE approaches the value of 185 MeV observed in binary fission (see dash-dotted line in Fig. 10). This behavior is different from the behavior of the values $\overline{\nu}$ and $\overline{E}_\gamma$, which saturated at $E_\alpha < 10$ MeV.

Table 1: Some characteristics of neutrons emitted in LCP accompanied fission

LRA			
$\overline{\nu}$	$E_\alpha < 10$ MeV $\overline{\nu}$	$E_\alpha > 10$ MeV $d\overline{\nu}/dE_\alpha$, MeV^{-1}	Ref.
3.11 ± 0.01	3.37 ± 0.02	-0.049 ± 0.002	*
3.13 ± 0.02		-0.037 ± 0.003	[24]
3.10 ± 0.08		-0.045 ± 0.010	[25]
3.11 ± 0.05		-0.026 ± 0.015	[26]
polar α			
$\overline{\nu}$		$d\overline{\nu}/dE_\alpha$, MeV^{-1}	Ref.
3.16 ± 0.07		-0.10 ± 0.03	*
	3.2 ± 0.2		*
tritons			
$\overline{\nu}$	$E_t < 7$ MeV $\overline{\nu}$	$E_t > 7$ MeV $d\overline{\nu}/dE_t$, MeV^{-1}	Ref.
2.90 ± 0.02	2.9 ± 0.1	-0.06 ± 0.02	*
2.95 ± 0.05		-0.039 ± 0.008	[24]
protons: $\overline{\nu} = 3.42 \pm 0.03$			*

* results of this work

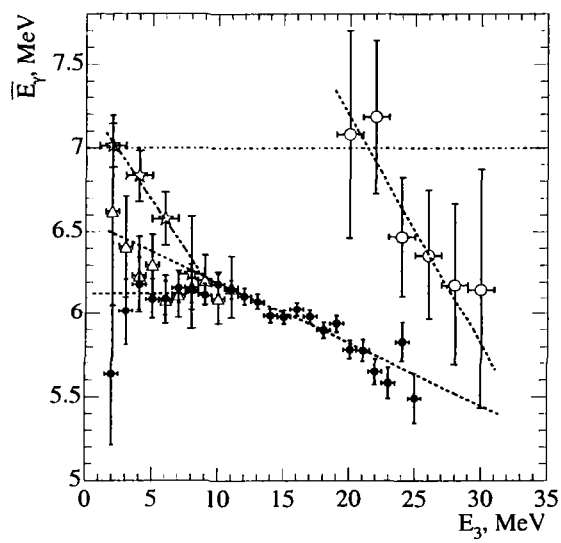

Figure 9: Dependence of the mean total energy of prompt γ-rays on the kinetic energy of ternary particles in LRA ($\bullet$), polar alpha ($\circ$), triton ($\triangle$), and proton ($\star$) accompanied fission.

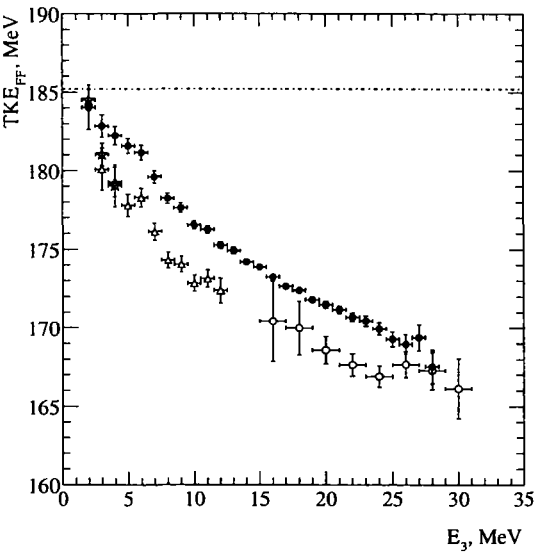

Figure 10: Dependence of the mean total kinetic energy of fission fragments on the kinetic energy of ternary particles in LRA (•), polar alpha (○), triton (△), and proton (⋆) accompanied fission.

3.1.8 Mass distribution of the fission fragments

The mass distribution of FFs in LRA accompanied fission is shown by the histogram in Fig. 11c. The mass distribution in binary fission is shown for comparison by the thin line. From such a comparison one can learn how the FFs contribute to the mass of ternary particles. From the shift of the light-fragment peak to smaller values observed in Fig. 11 one can conclude, that α-particles in ternary fission are produced at the expense of the mass of the light fission fragment. However, one should use this conclusion with caution, since our procedure of mass reconstruction is based on the E-E method, in which all three fragments are involved, therefore some possible methodical errors can not be excluded. A more reliable conclusion can be made in the frame of TOF-E method. Nevertheless, our conclusion is in good agreement with the result reported in recent works [12].

3.2 Triton accompanied fission

Let us consider now similar characteristics of triton accompanied fission. The energy spectrum of tritons selected by window "t" (see Fig. 1b) is shown in Fig. 12. Particles with energies larger than the punch-through energy were excluded from the analysis due to the applied selection condition. This results in a deficit of yield at the high-energy region of the energy spectrum. To compare with the data from the literature the yield of tritons was normalized to the yield of LRA.

The mean neutron multiplicity as a function of the triton kinetic energy is shown in Fig. 8 by opened triangles. In spite of not too high statistics one can conclude, that the evolution of $\overline{\nu}$ with E_t is qualitatively the same as in LRA accompanied fission. It is also

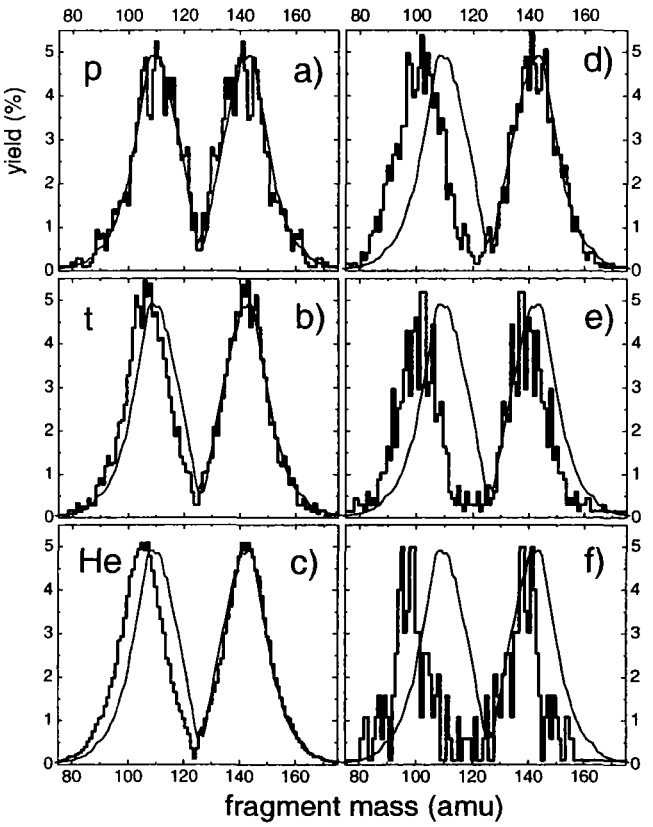

Figure 11: Mass spectra of FFs detected in coincidence with proton (a), triton (b), helium (c), Be-like fragment (d), C-like fragment (e), and fragments with mass of about ($15 < M_3 < 30$) amu (f); the thin line shows the mass distribution in binary fission.

clearly seen that the average neutron multiplicity in triton accompanied fission is always less than in alpha accompanied fission. The obtained value of mean neutron multiplicity for all selected events amounts to 2.90 ± 0.02.

The evolution of $\overline{E}_\gamma$ with the kinetic energy of the triton is shown in Fig. 9 by open triangles. $\overline{E}_\gamma$ does not differ very much from the value observed in LRA accompanied fission.

The angular distribution of tritons is shown in Fig. 22. The characteristics of the angular distribution are qualitatively similar to the characteristics observed for LRA accompanied fission. However, the width of the distribution seems to be somewhat broader than in LRA accompanied fission.

The mass distribution of FFs in triton accompanied fission is shown in Fig. 11b. One can conclude that mainly the light FFs contribute to the mass of triton. This conclusion, however, contradicts the conclusion of Ref. [27], where a shift of the heavy-fragment peak was reported.

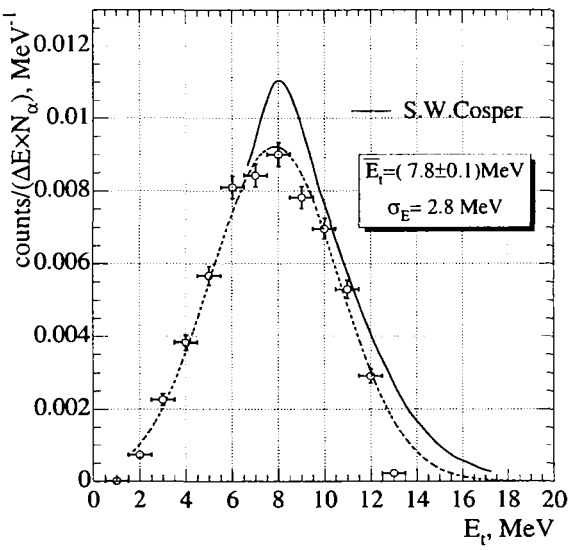

Figure 12: Energy spectrum of ternary tritons (o); the dashed line is the result of a Gaussian fit; the solid line is the result obtained by S.W.Cosper et al. [14]; the yields are normalized on the energy bin width and on the number of detected ternary α-particles.

3.3 Proton accompanied fission

The energy spectrum of protons stopped in Si-detectors is shown in Fig. 13 for $E_p \leq$ 7 MeV. At least two components are clearly seen, a low-energetic one with a maximum close to the low-energy threshold of Si-detectors (i.e. at $E_p \sim 2$ MeV), and a component at higher energies with a shoulder at $E_p \sim 6$ MeV. It was already observed in previous investigations (see, for instance, Refs. [14, 28]), that the proton energy spectrum is much more complicated than the energy spectra of other ternary particles. A considerable contribution to the total proton yield could come from background (n,p) reactions induced by fission neutrons. Careful analysis of contributions from different possible sources was done in Ref. [14, 28]. It was found that the component corresponding to protons emitted from ^{252}Cf during fission process has a Gaussian-like shape peaked at about 8 MeV. In our case the low-energy component could originate from Si(n,p) reactions inside the semiconductor detectors. At higher energies ($E_p \gtrsim 4$ MeV) the total energy spectrum (see Fig. 13) is a superposition of different hydrogen isotopes (but, still, mostly protons).

The angular distribution of protons is shown in Fig. 14. The difference in comparison with the angular distributions of other ternary particles is clearly seen. No strong focusing in the direction perpendicular to the fission axis is observed for detected protons. The angular distribution of prompt fission neutrons taken from [29] is also shown in Fig. 14 for comparison. It is quite well seen, that the shapes of both distributions are very similar.

The resemblance of the angular distributions of neutrons and protons indicates that the observed protons originate either from evaporation from FFs or from (n,p) reactions induced by fission neutrons. To analyze the contributions from various possible sources we calculated the energy spectra of protons and the results are shown in Fig. 15. The expected

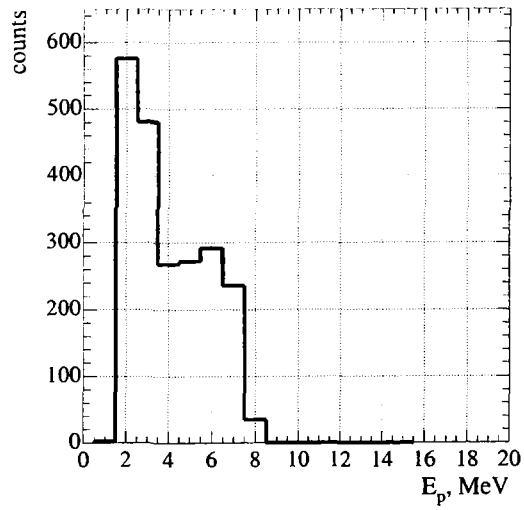

Figure 13: Energy spectrum of protons stopped in the Si-detector.

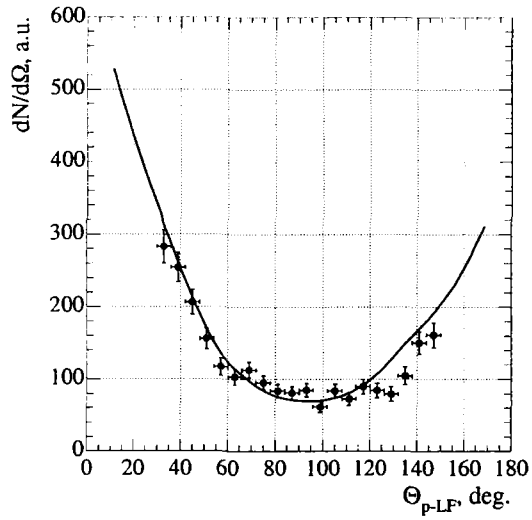

Figure 14: Distribution of angles between protons and light fission fragments (•); the solid line is the angular distribution of neutrons (taken from [29]).

energy spectrum of protons originating from (n,p) reactions in the silicon detectors is shown by histogram 1. To calculate the yield of protons from Si(n,p) reactions we used the information about the distribution of kinetic energies of prompt neutrons [29], and about the dependence of Si(n,p) reaction cross section on neutron kinetic energy [30]. The obtained value of proton yield from this source is $\approx 7 \times 10^{-5}$ with respect to binary fission or $\approx 2\%$ with respect to LRA yield. The expected distribution of *measured* kinetic energies of protons from ternary fission (histogram 2 in Fig. 15) was calculated assuming a Gaussian-like energy distribution of ternary protons centered at $E_p = 8$ MeV [14]. Let us remind that punch-through energy of protons in our case is ≈ 8 MeV, therefore the histogram 2 shows the distribution of ΔE. The sum of components 1 and 2 is shown in Fig. 15 by the dashed histogram, which qualitatively agrees with the experimental distribution shown by the filled histogram. Therefore, the measured spectrum can be understood taking into account above discussed two sources. However there is a small contradiction which should be mentioned. For events with protons from (n,p) reactions one should expect the neutron multiplicity on average to be one unit lower than in binary fission. As is seen from Fig. 8, the mean neutron multiplicity in the region of small proton energies amounts to $\overline{\nu} \approx 3.4$, which is much greater than the expected value of 2.77. For a more precise estimation one should use the information about the correlation between neutron multiplicity and neutron kinetic energy. However, it is unlikely that high neutron energies correspond to higher neutron multiplicities. Another possible reason of the discrepancy could be the contribution in the low-energy region from protons of ternary fission. However, in this case one should assume that the yield of this component is very high (at least 60% of the observed yield).

Let us turn to the analysis of protons from the high-energy region. If this component

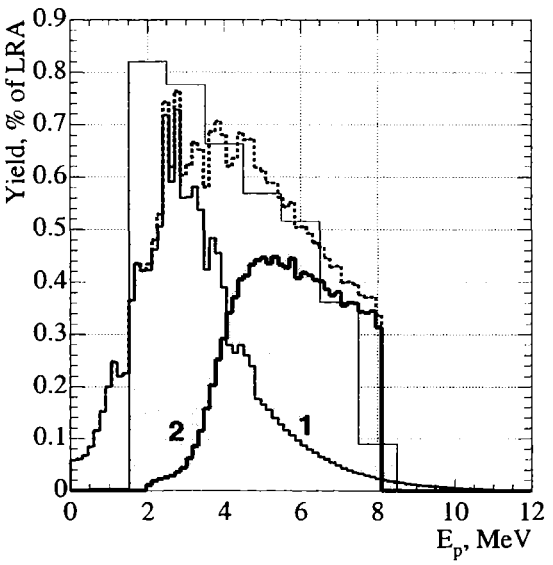

Figure 15: Proton yield with respect to LRA as a function of proton energy from Si(n,p) reactions (histogram 1, thin line) and from ternary fission (histogram 2, thick line); the dashed histogram is the sum of components 1 and 2; the filled histogram is the measured energy spectrum.

really originates from evaporation from FFs, than it would be interesting to get information about the evolution of the proton emission probability with the excitation energy of FFs. The multiplicity of emitted light particles can be used as a measure of excitation energy [3]. The ratio of the number of detected charged particles to the number of detected neutrons is demonstrated in Fig. 16 as function of total number of particles $N_{\rm lp}$ (number of neutrons plus a charged particle). In order to stress the difference between proton emission and emission of other CPs, the triton and alpha particles were counted as evaporative particles. It is clearly seen from the figure that the behavior of N_p/N_n ratio radically differs from the behavior of N_t/N_n and N_α/N_n ratios for tritons and equatorial α-particles. The increase of the N_p/N_n ratio with $N_{\rm lp}$ indicates an evaporative mechanism for the formation of the detected protons. The difference in the behavior of polar and equatorial α-particles also indicates in favor of the proposed method of analysis, because for evaporated α-particles one should expect a dependence of emission probability on excitation energy as well. The origin of low-energetic protons in Fig. 15 can be explained by proton emission in the direction opposite to the direction of the velocity of the FF.

3.4 Elastic scattering of fission fragments

The elastic scattering of FFs from binary fission on atomic nuclei contained in the materials of the target as well as the target backing contributes to ternary coincidences measured in the experiment. Therefore, one needs an effective method of discrimination of these events from events of ternary fission. The events of elastic scattering of FFs on the nuclei of the Ni-backing of the target are marked by the graphical cut "Ni" in Fig. 1b.

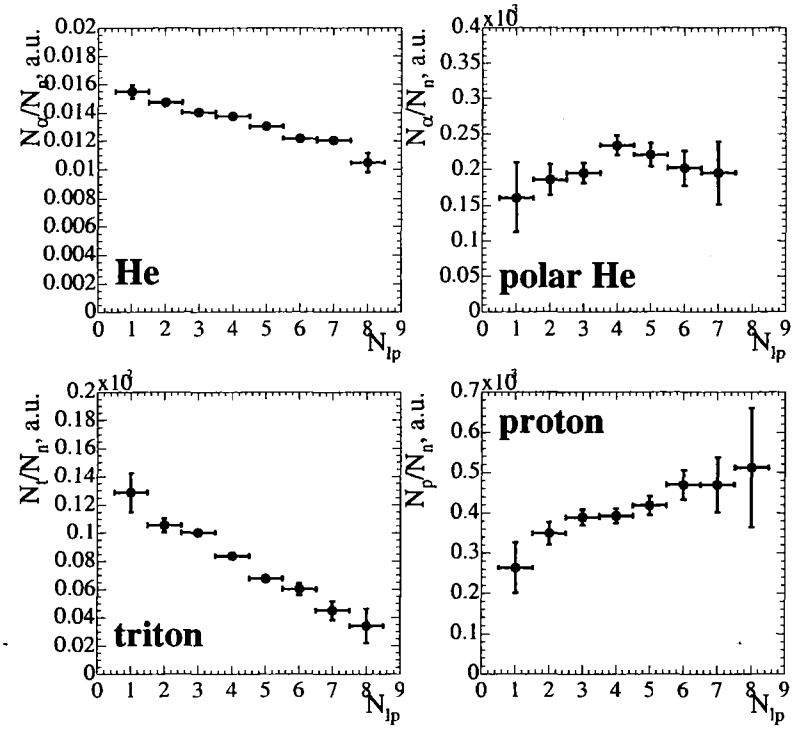

Figure 16: Ratio of the ternary charged-particle yield to the neutron yield as a function of the total number of emitted light particles.

These events can easily be discriminated from CPs originating from ternary fission, which is a big advantage of our experimental method. Let us consider some characteristics of these events, which will tell us how to discriminate against elastic scattering in future experiments.

The correlation between kinetic energy of recoiling Ni and the angle with respect to the light FF is shown in Fig. 17a. The highest yield of recoiling nuclei is observed in the lateral direction with respect to the fission axis. The main features of the observed correlation can easily be understood from classical consideration of the process of elastic scattering in inverse kinematic. The geometrical cross section of elastic scattering has a maximum for peripheral collisions and it decreases down to zero with decreasing impact parameter. In peripheral collisions nickel nuclei recoil at large angles with respect to the FF velocity vector and have small kinetic energies. In more central collisions the recoil angle is smaller whereas the recoil energy is higher. Such a correlation is well seen in Fig. 17. In most central collisions the recoil energy of the Ni nuclei could be even higher than the energy of scattered FFs. Therefore in such events it is difficult to distinguish between Ni and FFs. One should expect the mean neutron multiplicity to be independent of the kinetic energy of scattered Ni. Such a correlation is shown in Fig. 17b. Contrary to LCP accompanied fission, $\overline{\nu}$ is constant and equal to the value in binary fission.

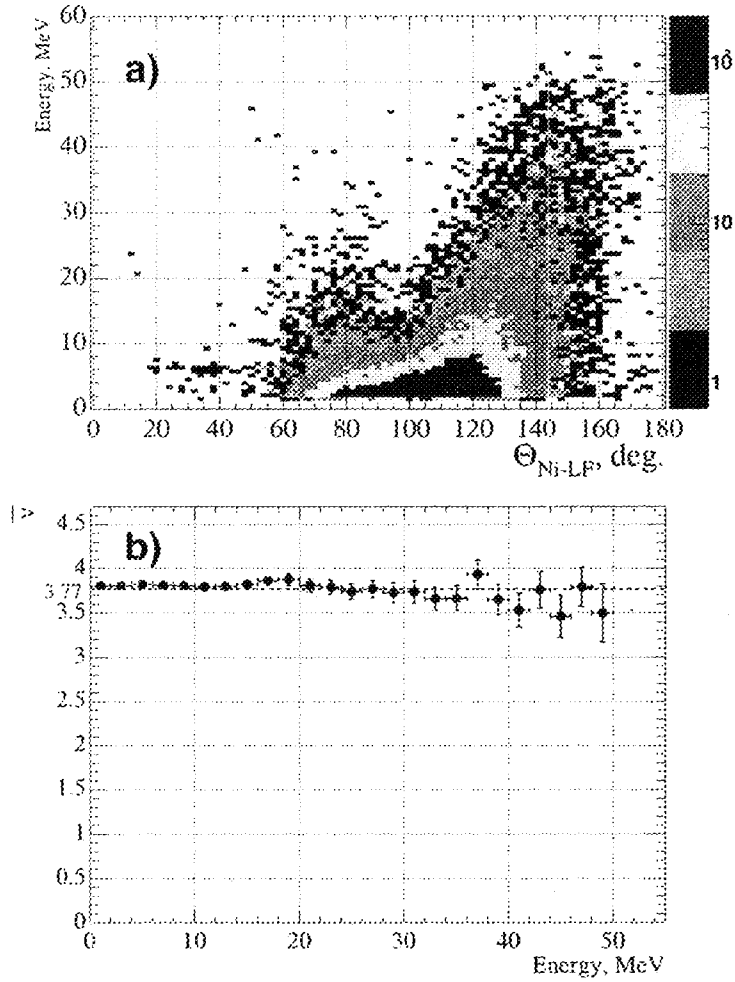

Figure 17: Correlation between the kinetic energy of scattered Ni nuclei and the angle of the Ni velocity vector with respect to the light fission fragment (a); the mean neutron multiplicity as function of the Ni kinetic energy (b).

3.5 IMF accompanied fission

In this paragraph we consider some characteristics of fission accompanied by emission of *intermediate mass fragments* (IMFs) conventionally defined as fragments with a charge greater than two and lighter than fission fragments. These particles are well seen in our data between the gates "He" and "Ni" (Fig. 1b). Unambiguous identification of various IMFs with the help of graphical selection conditions is not possible, therefore we will turn to the mass analysis. The distribution of mass M_3 calculated from parameters TOF_3 and E_3 is shown if Fig. 18 for all events from the region between windows "He" and "Ni" in Fig. 1. The increased yield at $M_3 \sim 10$ amu (presumably ^{10}Be) and in the region of $(12 \div 15)$ amu (presumably C) is well seen.

The energy spectrum of fragments with $(9 < M_3 < 11)$ amu is shown in Fig. 19. The

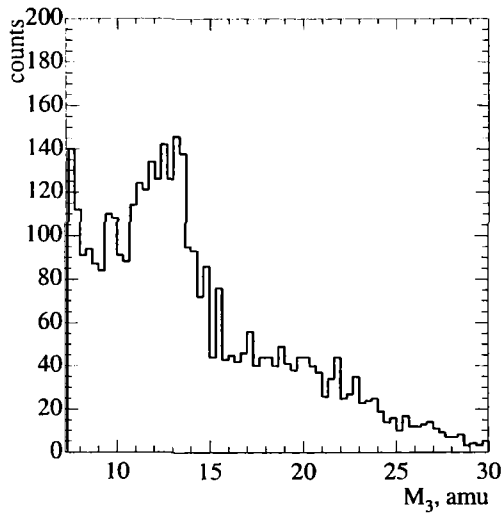

Figure 18: Mass distribution of IMFs in ternary fission.

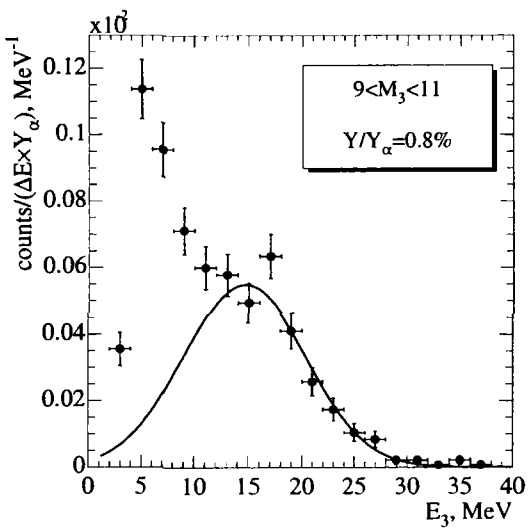

Figure 19: Energy distribution of ternary particles with mass $9 < M_3 < 11$ amu.

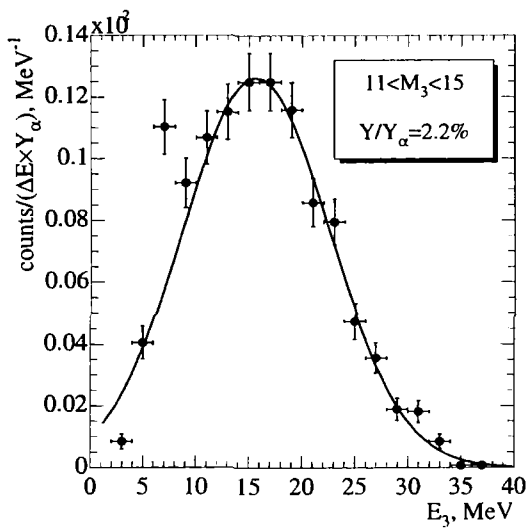

Figure 20: Energy distribution of ternary particles with mass $11 < M_3 < 15$ amu.

increased yield in the low-energy region can be explained by contribution from elastic scattering. The yield of events from ternary fission was estimated from a Gaussian fit (solid line) to the high-energy part of spectrum. However, the obtained value of about 0.8% with respect to LRA is higher than the yield of ^{10}Be reported in the literature.

Let us turn to the analysis of events with ternary particle mass from the region $(12 \div 15)$ amu. The correlation between particle energy and emission angle with respect to the light FF is shown in Fig. 21. At least two components are clearly seen, marked by graphical cuts 1 and 2. One can also see a third component which is similar to the component 2 concentrated symmetrically to the component 2 with respect to 90°, but of lower intensity.

Unambiguous selection of this component is not possible, therefore we will not analyze it separately. The shape of the component 2 is similar to the behavior observed for scattering on nickel nuclei (see Fig. 17). The correlation of the component 1 on the contrary is more similar to the correlation observed in LCP accompanied fission (see Fig. 5). We suppose that the component 2 is due to elastic scattering of *heavy* FFs on carbon nuclei contained in the target materials, whereas events in window 1 correspond to events of ternary fission. Events corresponding to elastic scattering of *light* FFs produce the third component of considerably lower intensity mentioned above. To verify this hypothesis we analyzed neutron data for both components. The dependence of $\overline{\nu}$ on the kinetic energy of the ternary particle is shown in Fig. 21b. It is well seen that the neutron multiplicity for events from window 2 is independent of the particle energy and is equal to the value in binary fission (see Fig. 17b). The neutron multiplicity for events from window 1 is smaller than in binary fission and it decreases with increasing particle kinetic energy. A similar behavior was observed for LRA and triton accompanied fission (Fig. 8). At low kinetic energies ($E_{IMF} < 8$ MeV) the deduced value of $\overline{\nu}$ is largely due to the contamination by events of elastic scattering.

The energy distribution of events from window 1 is analyzed in Fig. 20. The maximum of the distribution is at about 16 MeV. This value is very close to the value observed for He and Be fragments. The increased yield at low energies is due to the above discussed component of elastic scattering. The Gaussian fit of the experimental points (the solid line in the figure) was made by using only events with $E_{\mathrm{IMF}} > 10$ MeV.

The estimated yield of ternary carbon-like fragments amounts to about 2% of LRA yield. This value is considerably higher than the value reported in the literature. The reason of the difference could be explained by very high energy threshold (> 20 MeV) in previous investigations. The obtained value of the yield of carbon-like fragments is unexpectedly high, higher than the yield of the lighter Be nuclei and therefore in contradiction with the existing systematics (see, for instance, Ref. [21]).

The analysis of events with ternary particle mass of $(16 \div 30)$ amu is carried out in the same manner as in the previous case. The estimated yield of IMFs in this region is about 0.7% of the LRA yield.

The angular distributions of IMFs selected by window 1 (see Fig. 21a) is shown in Fig. 22. No corrections for the finite size of Si-detectors has been applied.

The dependence of the neutron multiplicity on the kinetic energy of ternary particles is demonstrated in Fig. 23. The common tendency of decreasing neutron multiplicity with increasing particle kinetic energy is quite well seen.

The mass distributions of FFs in fission accompanied by emission of IMFs are shown in Fig. 11d-f. One can conclude that mostly the light FF contributes to the formation of IMF. An interesting feature of the mass distributions concerns the position of heavy-fragment peak (Fig. 11f). The distribution is peaked at ~ 140 amu and the width of the distribution is quite narrow.

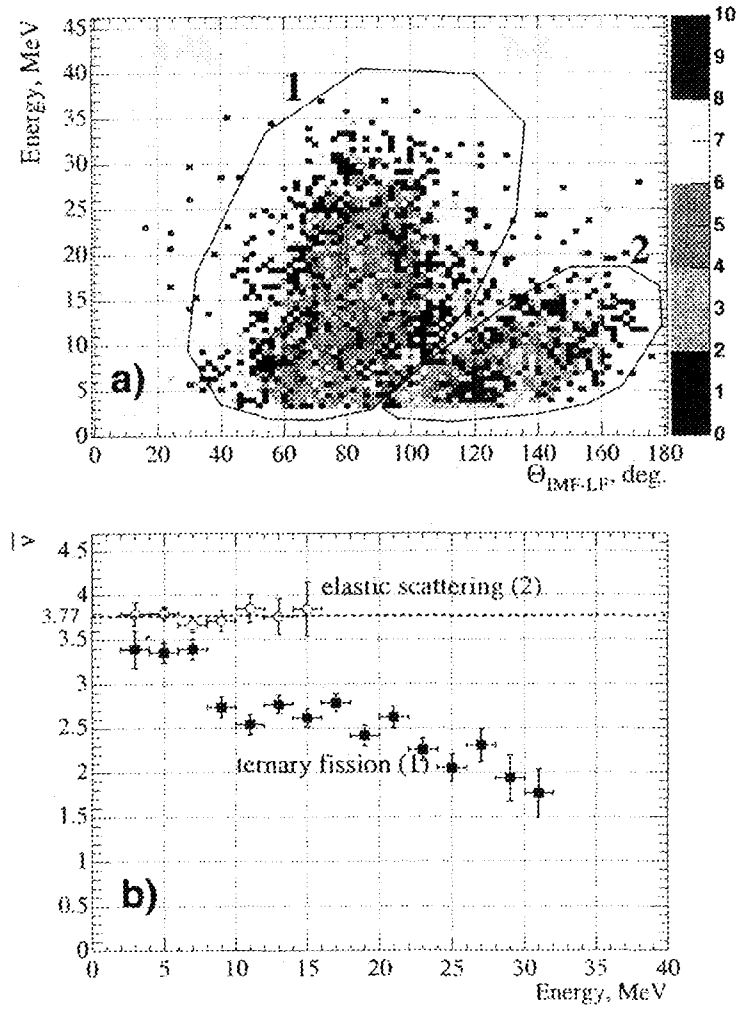

Figure 21: (a) Correlation between kinetic energy and emission angle with respect to the light FF of IMFs with masses in the region $(12 \div 15)$; (b) mean neutron multiplicity as function of the ternary particle kinetic energy for two selection windows, window 1 (■) and window 2 (○).

3.6 True ternary fission?

Events from window 1 in Fig. 1 are of special interest because fragments from mass-symmetric decays are expected to fall into this region. Unfortunately, this region is polluted by events of elastic scattering, therefore the separation of possible events of true ternary fission is not possible in the frame of present experiment. The average multiplicity of associated neutrons amounts to 3.5 ± 0.1 which is somewhat less than the value observed in binary fission, but still rather high for making definite conclusions.

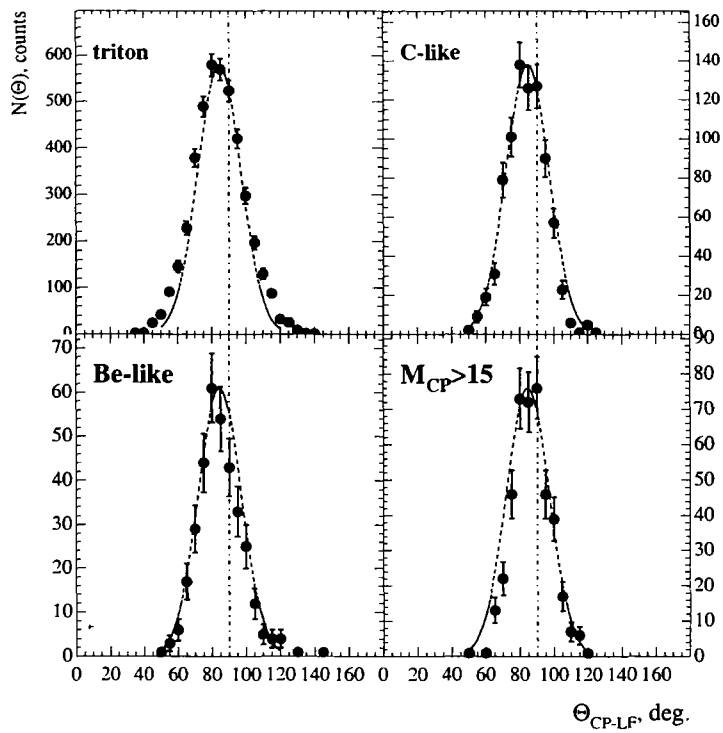

Figure 22: Distribution of angles between the ternary particles and the light fission fragments; the dashed line is the angular distribution of α-particles approximated with a Gaussian.

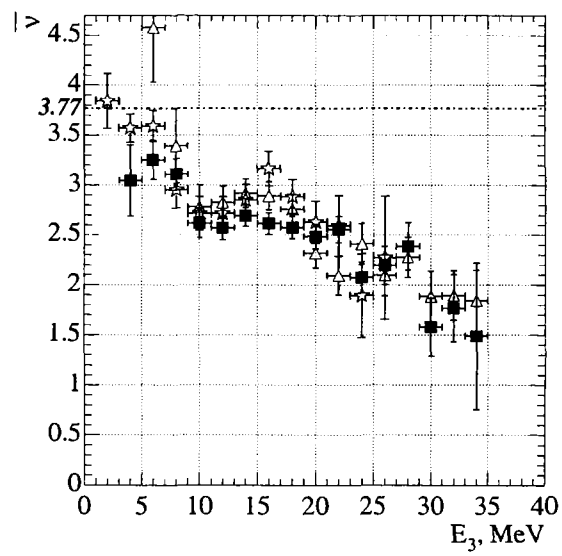

Figure 23: Mean neutron multiplicity as function of the kinetic energy of the ternary particle, $9 < M < 11$, ($\star$) $11 < M_3 < 15$ (■), $15 < M_3 < 30$ (△)

Table 2: Some characteristics of events detected with multiplicity three.

detected particle	No. of det. particles	Extrapo-lated	$\overline{\nu}$ (energy range, MeV)	$\overline{E}$ MeV	N/N_α %
p(+d+t)	3214		3.43 ± 0.03 (> 2)		3.8
t	5240	5508	2.90 ± 0.02 ($2 \div 12$)	7.8 ± 0.1	6.4*
α	85560		3.11 ± 0.01 (> 2)	15.8 ± 0.1	100
$9 < M_3 < 11$		684	2.9 ± 0.1 (> 10)	15 ± 2	0.8*
$11 < M_3 < 15$		1882	2.5 ± 0.1 (> 10)	15.6 ± 0.2	2*
$15 < M_3 < 30$		590	2.1 ± 0.2 (> 20)	25 ± 2	0.7*
$Ni_{el.scat.}$	62141		3.81 ± 0.01 (> 2)		73

* extrapolated value used

3.6.1 Random coincidences

The main feature of events selected by window 2 in Fig. 1b is the high kinetic energy of all detected fragments. The average multiplicity of associated neutrons amounts to $\overline{\nu} = 8.4$. Consequently, we can conclude that these events originate from random coincidences of FFs from two events of binary fission.

3.7 Summary

Some characteristics of detected ternary events are summarized in Table 2. The number of events corresponding to the selection condition is given in the second column. The corrected number of particles obtained by extrapolation is shown in third column of the table. The extrapolation was made using results of a Gaussian fit of the corresponding energy distribution. The value of the mean neutron multiplicity is presented in the fourth column. The corresponding range of kinetic energy of the ternary particle used for multiplicity determination is given in brackets. The mean kinetic energy of ternary particles obtained from the Gaussian fit of energy distribution is shown in fifth column. The yield of ternary particles with respect to the yield of LRA is presented in the last column of the table. The yield of tritons is slightly less than the value reported in other investigations. It is not surprising because we cannot be sure that we extrapolated correctly to the unobserved high-energy region of the energy spectrum. However, the total yield of all hydrogen isotopes excluding low-energy part of protons amounts to $N_H/N_\alpha = (9.5 \pm 0.5)\%$ which agrees quite well with the value of 9.3% reported in [12].

One can see from the table that the yield of events of elastic scattering is very high. It amounts to more than 70% of the yield of ternary α-particles. This demonstrates that the task of elastic scattering discrimination is of great importance in experiments aimed at the search of rare decay modes.

Neutron multiplicity distributions not corrected for neutron detection efficiency are shown in Fig. 24. The most probable value of the neutron multiplicity is always greater than zero irrespective of the ternary particle type. Fission fragments are, therefore, highly

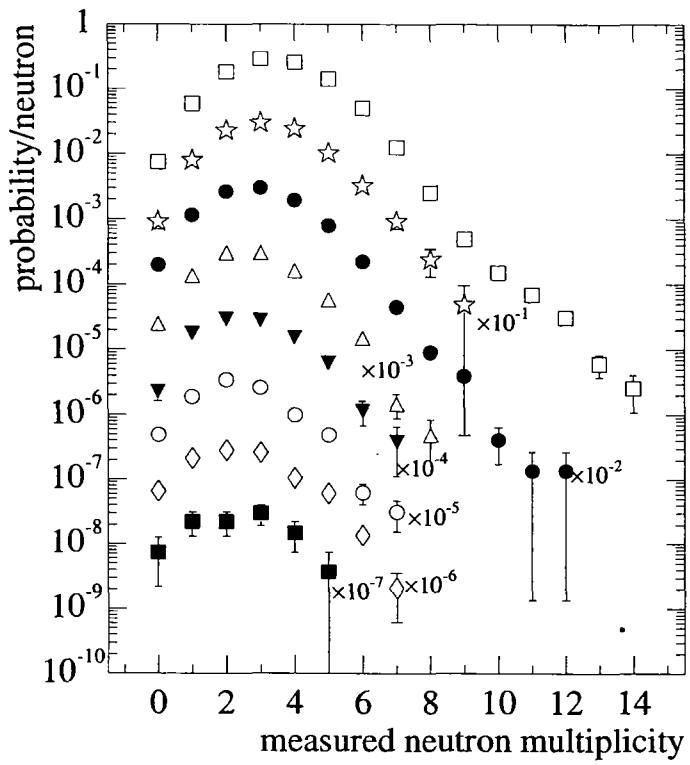

Figure 24: Neutron multiplicity distributions in binary fission (□), fission accompanied by emission of proton (⋆), LRA (•), triton (△), Be-like nuclei (▼), C-like nuclei (○), nuclei with mass (15 ÷ 30) amu (◇), and two α-particles (■).

excited even in the case of emission of heavy ternary particles.

4 Quaternary fission

In this section we analyze events with four detected CPs. The correlation between kinetic energy of CP and time-of-flight calculated by formula 1 is shown in Fig. 25. For particle identification we use graphical cuts defined during the analysis of ternary data (see Fig. 1b). Contributions from events of scattering of FFs on Ni and C or O nuclei are well seen in Fig. 25. The highest number of detected coincidences is due to α-α coincidences. Several events of α-t and α-p coincidences were also detected. In the next paragraphs we will discuss the characteristics of these decays in more detail. Events of fission accompanied by higher particle multiplicity have not been detected within the statistical level of 10^{-7} with respect to binary fission.

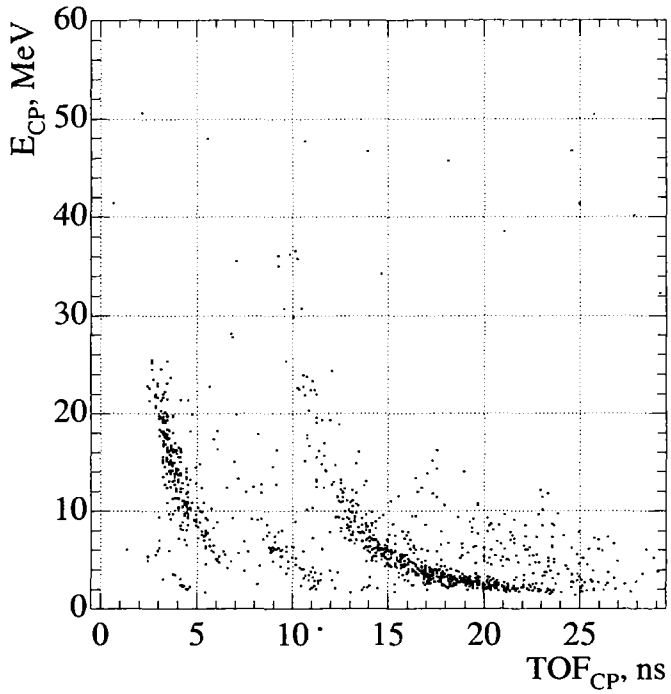

Figure 25: Correlation between kinetic energy and time-of-flight calculated by formula (1) of CPs in quaternary fission.

4.1 α-α correlations

The total number of detected α-α coincidences amounts to 34. The energy spectrum of α-particles is compared in Fig. 26 with the energy spectrum of ternary LRA. The mean kinetic energy of α-particles in quaternary fission is less than in ternary fission. Such a difference is also reported in Ref. [32]. The distribution of angles between the velocity vector of α-particles and the velocity vector of light FFs is compared in Fig. 27 with similar distributions observed in ternary fission. It is quite well seen, that quaternary α-particles are focused perpendicular to the fission axis. This indicates that α-particles originate from the neck-zone of fissioning nucleus similar to CPs in ternary fission. To study the correlations between α-particles we plot in Fig. 28 the distribution of angles between projections of α-particle velocities on a plane perpendicular to the velocity vector of light FFs ($\phi_{\alpha-\alpha}$). This coordinate system was chosen in order to reduce the effect of simultaneous deflection of both particles by the heavy FF. However, the result is very similar to the result obtained by using the angles between velocities. It is quite well seen from the figure that the angle between projections is less than 90° for most of the events. This indicates the correlation between two α-particles. For uncorrelated particles one should expect a uniform distribution. It would be interesting to analyze the observed correlation in more detail because from this analysis one can deduce information about the source of particles or about the properties of the zone from which particles where emitted. In principle, the detected α-α coincidences could originate from the decay of

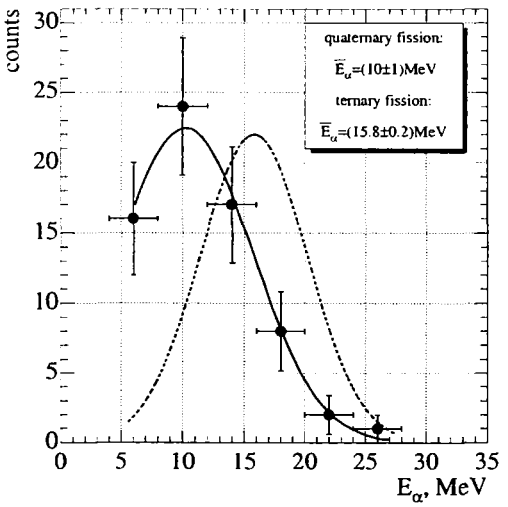

Figure 26: Energy distribution of quaternary α particles (•); the solid line is the result of a Gaussian fit; the dashed line gives the energy distribution of α-particles in ternary fission.

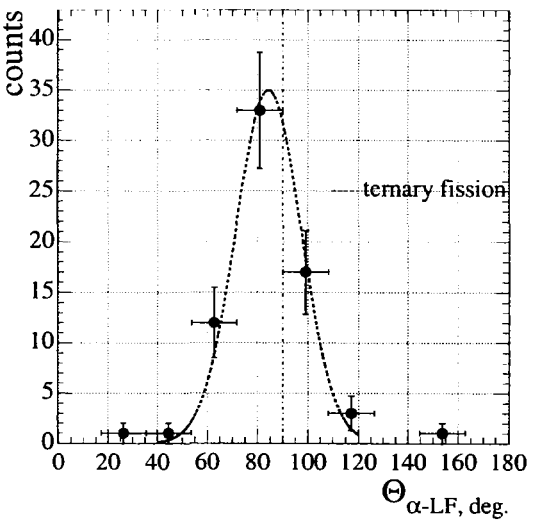

Figure 27: Distribution of angles between the α-particle and the light fission fragment in quaternary (symbols) and ternary (dashed line) fission.

ternary ^{8}Be into two α-particles. In this case the maximum angle between two α-particles is $\Theta_{max} = 2\arctan(\sqrt{Q/E_{Be}})$, where Q is the reaction Q-value and E_{Be} is the kinetic energy of Be nucleus. The angle between two alpha particles originating from the decay of ^{8}Be nucleus in the ground state is about 8° assuming $E_{Be} = 16$ MeV ($Q = 94$ keV). The detection efficiency for events of such a type is about $\varepsilon \approx 0.3$. If ^{8}Be decays from the first excited state ($E^* = 2.9$ MeV), then $\Theta_{max} \approx 46°$ and the corresponding detection efficiency is $\varepsilon \approx 0.5$. Therefore, most of the detected events can be associated with the ^{8}Be decay, but there are three events with a relative angle between α-particles greater than 90°, which could originate from true quaternary fission. Another important observable which can help to distinguish between different sources is the relative velocity of two particles. This observable is independent of the velocity of the source and it is determined only by the energy released in the decay. The distribution of relative velocities is shown in Fig. 29. It is possible to distinguish three regions centered at 0.8, 2.5, and 5 cm/ns, respectively. The first two regions most probably correspond to the decay of ^{8}Be from ground and first excited state, respectively. The relative velocity of two α-particles in the case of ^{8}Be decay from the ground state should be $V_{rel} \approx 0.15$ cm/ns. The difference with experimental value can be easily explained taking into account the finite size of our semiconductor detectors. We ascribe to particles with a small relative angle the coordinates corresponding to the centers of the hit detectors. This increases the measured value of the relative angle between the particles, and, hence, the value of the reconstructed relative velocity. The events at about 5 cm/ns cannot be explained by the decay of ^{8}Be nuclei. These events originate most probably from true quaternary decay of ^{252}Cf.

To reconstruct the velocity of the source of α-particles we show in Fig. 30 the distribu-

tion of velocities of the center-of-mass of α-particles. The distribution is peaked at about 2.1 cm/ns. Assuming that the ^{8}Be nucleus moves with this velocity we can calculate its kinetic energy, $E_{Be} = 18$ MeV. This value is close to the kinetic energy of Be-like nuclei observed in ternary fission (see Table 2). The small difference is not surprising because one can expect that ^{8}Be can gain higher kinetic energy than ^{10}Be due to the smaller mass.

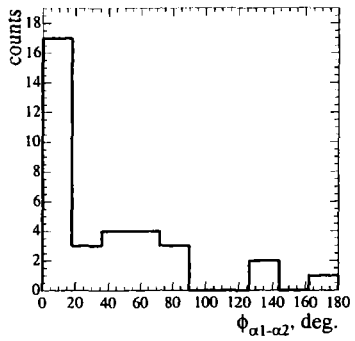

Figure 28: Distribution of angles between projections of α-particle velocities on a plane perpendicular to the velocity of the light fission fragment.

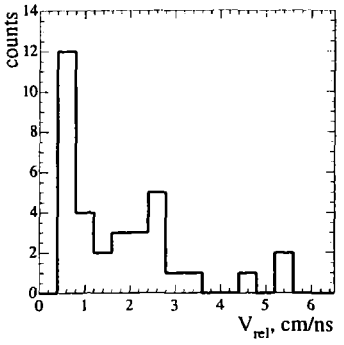

Figure 29: Distribution of relative velocities between two α-particles.

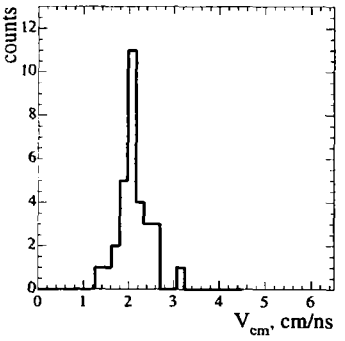

Figure 30: Distribution of the velocities of the center-of-mass of the two α-particles.

In spite of low statistic we analyzed some characteristics of events in regions defined above and the results a summarized in Table 4. First of all, the anticorrelation between the total kinetic energy of α-particles TKE_α and the mean neutron multiplicity is well seen. This is a good indication of the genetic relation of detected particles. One should expect a decrease of the neutron multiplicity in the case of ^{8}Be decay from the excited state with respect to the decay from the ground state taking into account total energy balance (assuming, of course, that other components of energy balance are the same in both decay modes). The expected decrease of neutron multiplicity is $\Delta\overline{\nu} \approx 0.6$, using neutron binding energy of 5.2 MeV. This value is in agreement with the observed difference of 0.7 ± 0.4 between components 1 and 2. The mean total kinetic energy of α-particles of the third component is close to twice the mean kinetic energy of ternary α-particles. These events are accompanied by low neutron multiplicity. The characteristics of these events are consistent with the assumption that these particles originate from quaternary decay. The collected statistics is unfortunately not sufficient to make further analysis. Therefore, experiments with higher statistics could be a good task for future investigations with the NESSI detector.

4.2 α-t correlations

Five events of α-t coincidences were detected. In spite of too low statistics we will try to analyse some characteristics of the decay mechanism.

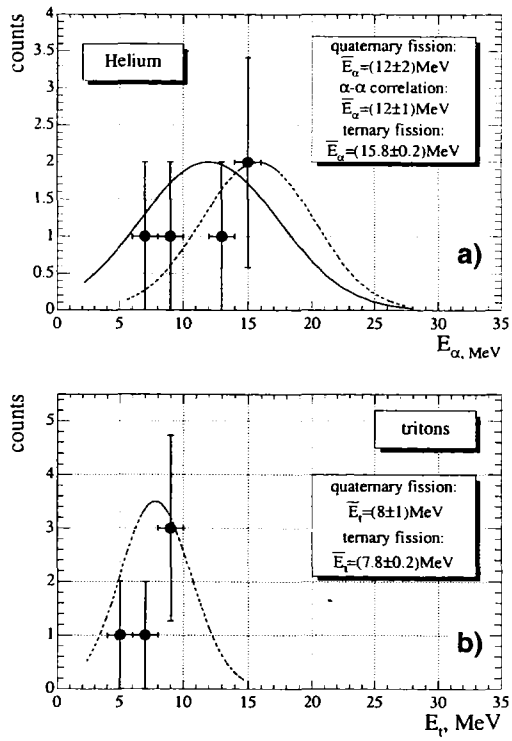

Figure 31: Energy distribution of quaternary α-particles (a,•) and tritons (b,•); the solid line is the energy distribution of quaternary α-particles in α-α correlation; the dashed line is the energy distribution of particles in ternary fission.

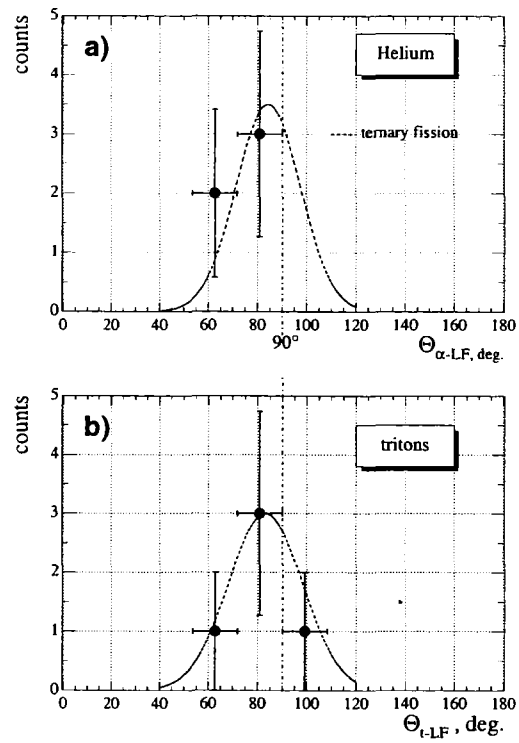

Figure 32: Angular distribution of quaternary α-particles (a,•) and tritons (b,•) with respect to the light fission fragment; the dashed line is the angular distribution of particles in ternary fission.

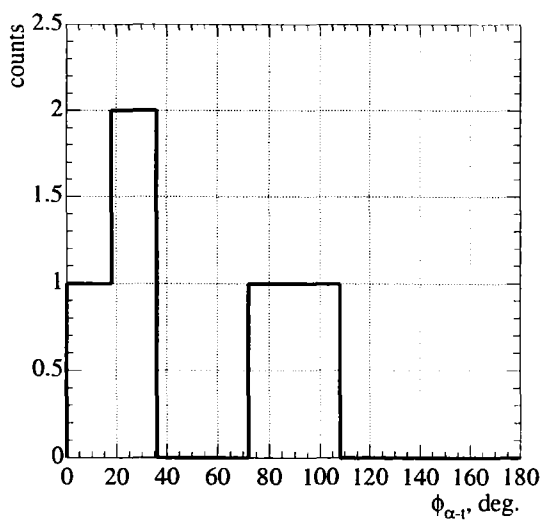

Figure 33: Distribution of angles between the projections of α-particle and triton velocities on plane perpendicular to the velocity of light fission fragment.

The energy distributions of the detected particles are shown in Fig. 31. The mean kinetic energy of α-particles is similar to the value observed in α-α correlations. The mean kinetic energy of tritons seems to be similar to the value observed for ternary tritons. From the angular distributions one can conclude that both particles are focused in lateral direction with respect to the fission axis (see Fig. 32). The tendency observed in the distribution of the angles $\phi_{\alpha-t}$ (Fig. 33) indicates a possible correlation of the particles.

4.3 α-p correlations

Eight events of α-p coincidences were detected. The mean energy of α-particles (see Fig. 34a) is very similar to the value observed in ternary fission. In the proton energy spectrum (see Fig. 34b) only the low-energy component exists (compare with Fig. 13). Alpha particles are emitted perpendicular to the fission axis (see Fig. 35a), whereas the angular distribution of protons (see Fig. 35b) is similar to the angular distribution ob-

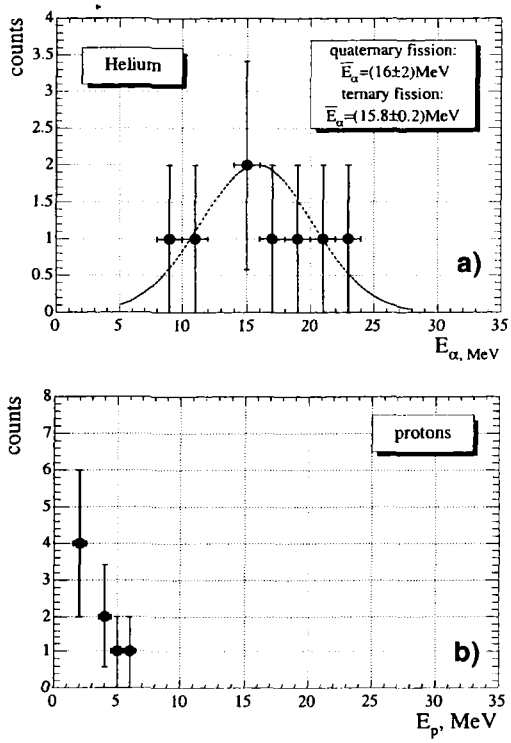

Figure 34: Energy distribution of quaternary α-particles (a,•) and protons (b,•); the dashed line is the energy distribution of particles in ternary fission.

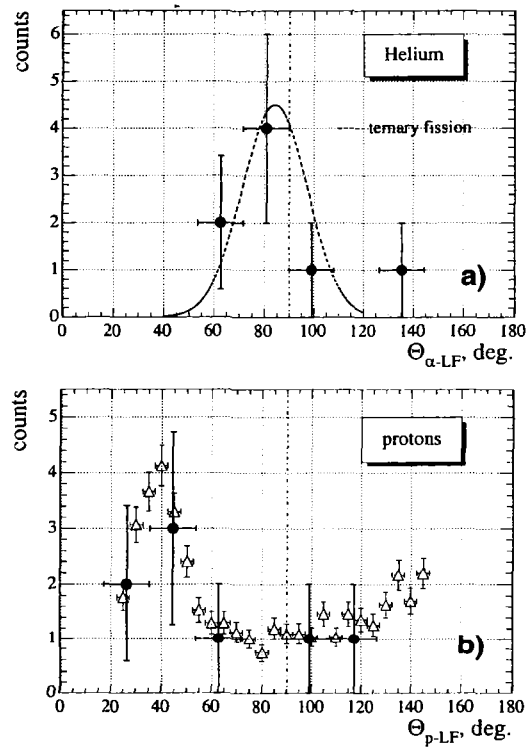

Figure 35: Angular distribution of quaternary α-particles (a,•) and protons (b,•) with respect to the light fission fragment direction; the dashed line is the angular distribution of α-particles in ternary fission; triangles show the angular distribution of ternary protons.

served for events with multiplicity 3 (see Fig. 14). Angles $\phi_{\alpha-p}$ seem to be uniformly distributed. From these characteristics we conclude, that the detected events are most probably due to the coincidence of a ternary LRA and a proton emitted from a FF or a proton from the (n,p) reaction.

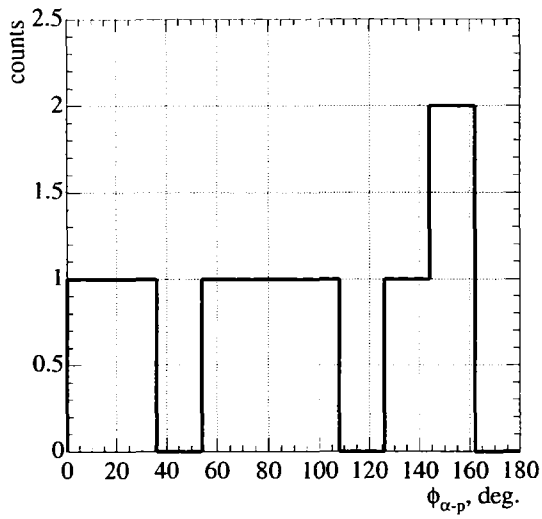

Figure 36: Distribution of angles between the projections of α-particle and proton velocities on plane perpendicular to the velocity of the light fission fragment.

4.4 The yield

The detection efficiency for events with multiplicity four was obtained from Monte Carlo simulation. The obtained value amounts to $\varepsilon = 0.5 \div 0.6$ depending on the assumptions about the distribution of various observables. The summary of yields obtained employing $\varepsilon = 0.55$ is given in Table 3. The yield of components 1 and 2 in Table 4 was estimated using $\varepsilon = 0.3$ and $\varepsilon = 0.5$, respectively.

Table 3: Some characteristics of events detected with multiplicity four.

	No. of det. events	$\overline{\nu}$	$\overline{E}$, MeV	N/N_{binary}
α-α	34	2.4 ± 0.2	10 ± 1	$(1.5 \pm 0.4) \times 10^{-6}$
α-p	8	2.8 ± 0.5	$16 \pm 2 \quad 3 \pm 1$	$(0.4 \pm 0.2) \times 10^{-6}$
α-t	5	3.5 ± 0.6	$12 \pm 2 \quad 8 \pm 1$	$(0.2 \pm 0.1) \times 10^{-6}$

Table 4: Some characteristics of events in α-α coincidences.

	V_{rel} cm/ns	No. of events	$\overline{\nu}$	$\overline{TKE_\alpha}$, MeV	N/N_{binary}
1	$0 \div 1.5$	18	3.0 ± 0.3	20 ± 1	1.5×10^{-6}
2	$1.5 \div 3.5$	13	2.3 ± 0.3	26 ± 2	0.6×10^{-6}
3	$4 \div 6$	3	1.2 ± 0.6	34 ± 5	0.1×10^{-6}

5 Summary

Ternary and quaternary spontaneous decay of ^{252}Cf was studied using two 4π detectors for charged particles, γ-rays and neutrons. The method of fragment identification based on the measurements of kinetic energies and relative time-of-flights of the decay products has been successfully tested. The main advantages of the employed approach in comparison with other experimental methods used in earlier experiments are:

1. Due to the lack of a start-detector the largest possible solid angle is available for fragment detection.

2. The high geometrical efficiency thus achieved allows to investigate rare decays with a weak source without the use of absorption foils to protect detectors from irradiation by α-particles from natural α-decays of ^{252}Cf.

3. The lack of a start detector and absorption foils decreases considerably the threshold in comparison with other experiments.

4. Employment of time as a parameter for fragment identification reduces considerably the contribution from random coincidences with α-particles from natural α-decay of ^{252}Cf.

The comparison of characteristics of LRA accompanied fission with well-known data from the literature shows a good quality of the data collected in the frame of the new approach.

A wide range of ternary particles from protons up to $M_3 \sim 30$ amu has been covered. Our experiment demonstrates that the elastic scattering of FFs produces a strong background to the ternary fission data. Fortunately, the elaborated approach allows to reject carefully the events of elastic scattering. Unfortunately, these events contaminate greatly the region where the events of true ternary fission are expected. As to the investigation of *true ternary fission* the Cf-source on a nickel backing is therefore certainly not a good choice.

The NESSI detector was found to be well-suited for the study of quaternary fission as well. In spite of low statistics some characteristics of these rare decay modes have been analyzed and compared with ternary fission. The characteristics of α-t and α-α quaternary decays were found to be very similar. All particles are focused in lateral direction with

respect to the fission axis similar to ternary particles. Strong focusing effects indicate that these particles originate from the neck-zone of the fissioning nucleus. The angular distributions indicate the existence of correlation between particles. The mean kinetic energies of quaternary particles are similar to the kinetic energies of ternary particles, but somewhat smaller. Detected α-p coincidences exhibit essentially another characteristics. In this decay mode α-particles are focused perpendicular to the fission axis, but the angular distribution of protons is more isotropic and similar to the angular distribution of protons in threefold coincidences. Most likely, the α-p coincidences originate from the coincidence of an α-particle from ternary fission and a proton emitted by a fission fragment or a proton from (n,p) reactions induced by fission neutrons in a Si-detector. The highest number of detected coincidences is due to α-α coincidences (70%). These coincidences were analyzed in more detail due to higher statistics. It was found, that most of the detected events can be explained by the decay of a ^{8}Be nucleus from the ground and the first excited states. Three events where detected which cannot be explained by the ^{8}Be decay. They originate most likely from true quaternary fission of ^{252}Cf. The estimated yield of these events is $\approx 10^{-7}$ with respect to binary fission. For a more detailed analysis we are planning to collect higher statistics with a stronger ^{252}Cf-source. According to our estimate we can increase the intensity of the source at least by factor of 10 without any danger to overload our experimental facility with high counting rates.

Finally we conclude, that the NESSI detector, the unique combination of two 4π detectors for charged particles, neutrons and γ-rays, is a highly effective tool for the investigation of nuclear fission accompanied by the emission of charged particles and true ternary fission. To our knowledge, it is the first time that such a rich information about the characteristics of various decay modes was obtained within a single experiment.

References

[1] L.W. Alvarez as reported by G. Farwell, E. Segrè, C. Wiegand, Phys. Rev. **71**, 327 (1947).

[2] H.-G. Ortlepp, W. Wagner, C.-M. Herbach *et al.*, Nucl. Instrum. Methods **A 403**, 65 (1998).

[3] M. Enke, C.-M. Herbach, D. Hilscher *et al.*, Nucl. Phys. **A 657**, 317 (1999).

[4] O. Hahn and F. Strassmann, Naturwiss. **27**, 11 (1939).

[5] R.D. Present, Phys. Rev. **59**, 466 (1941).

[6] H. Diehl and W. Greiner, Phys. Lett. **B 45**, 35 (1973).

[7] H. Diehl and W. Greiner, Nucl. Phys. **A 229**, 29 (1974).

[8] P. Schall, P. Heeg, M. Mutterer, J.P. Theobald, Phys. Lett. **B 191**, 339 (1987).

[9] D. Hilscher, U. Jahnke, F. Goldenbaum *et al.*, Nucl. Instrum. Methods **A 414**, 100 (1998).

[10] P. Figuera, W. Bohne, B. Drescher *et al.*, Z. Phys. **A 352**, 315 (1995).

[11] S.I. Mulgin, V.N. Okolovich, S.V. Zhdanov, Nucl. Instrum. Methods **A 338**, 254 (1997).

[12] C. Wagemans, *The Nuclear Fission Process*, CRC Press, Boca Raton, 1991.

[13] W. Loveland, Phys. Rev. **C 9**, 395 (1974).

[14] S.W. Cosper, J. Cerny, R.C. Gatti, Phys. Rev. **154**, 1193 (1967).

[15] D.E. Cumpstey and D.G. Vass, in: *Physics and Chemistry of Fission 1979*, Proc. of an Int. Symp. held at Jülich, May 14-18, 1997, IAEA-SM-241, Vienna, 1980, vol. 1, p.223.

[16] G.A. Pik-Pichak, Sov. J. Jad. Phys. **40**, 336 (1984).

[17] N.A. Perfilov and Z.I. Solovieva, Sov. Phys. JETP **10**, 824 (1960).

[18] Z. Fraenkel, Phys. Rev. **156**, 1283 (1967).

[19] D.M. Nadkarni, S.K. Kataria, S.S. Kapoor, P.N. Ramo Rao, Nucl. Phys. **A 196**, 209 (1972).

[20] M.J. Fluss, S.B. Kaufman, E.P. Steinberg, B.D. Wilkins, Phys. Rev. **C 7**, 353 (1973).

[21] I. Halpern, Annu. Rev. Nucl. Sci. **21**, 245 (1971).

[22] E. Piasecki and L. Nowicki, in: *Physics and Chemistry of Fission 1979*, Proc. of an Int. Symp. held at Jülich, May 14-18, 1997, IAEA-SM-241, Vienna, 1980, vol. 2, p.193.

[23] G.K. Mehta, J. Poitou, M. Ribrag, C. Signarbieux, Phys. Rev. **C 7**, 373 (1973).

[24] H. Hongyin, H. Shengnian, M. Jiangchen *et al.*, in: J.W. Behrens and A.D. Carlson (Eds.), Proc. of *Fifty years with nuclear fission*, National Academy of Sciences, Washington, D.C., and National Institute of Standards and Technology, Gaithersburg, Maryland, U.S.A, April 25-28, 1989, published by American Nuclear Society, 1989, ISBN/ISSN 0894481444, vol.2, p.684.

[25] H. Piekarz, J. Blocki, T. Krogulski, E. Piasecki, Nucl. Phys. **A 146**, 273 (1970).

[26] E. Nardi and Z. Fraenkel, Phys. Rev. **C 2**, 1156 (1970).

[27] M. Mutterer, P. Singer, Yu. Kopach *et al.*, in: J. Kliman and B. I. Pustylnik (Eds.) *Dynamical aspects of nuclear fission*, Proc. of 3-rd Int. Conf., Častá-Papernička, Slovak Republic , August 30 - Sept. 4, 1996, JINR, E6,7-97-49, Dubna, Russia, 1997, p.250

[28] J.A. Adams and R.R. Roy, Nucl. Sci. and Eng. **63**, 41 (1977).

[29] H.R. Bowman, S.G. Thompson, J.C.D. Milton, W.J. Swiatecki, Phys. Rev. **126**, 2120 (1962).

[30] http://t2.lanl.gov.

[31] J.F. Wild, P.A. Baisden, R.J. Dougan *et al.*, Phys. Rev. **C 32**, 488 (1985).

[32] S.K. Kataria, E. Nardi, S.G. Thompson, in: *Physics and chemistry of fission 1973*, Proceedings of the 3rd IAEA Symposium on the physics and chemistry of fission held by the IAEA in Rochester, New York, 13-17 August 1973, IAEA-SM-174, Vienna, 1974, vol. 2, p.389.